Atmos. Chem. Phys., 23, 183–201, 2023
https://doi.org/10.5194/acp-23-183-2023

Atmospheric Chemistry and Physics
Open Access
EGU

Measurement report: Atmospheric new particle formation at a peri-urban site in Lille, northern France

Suzanne Crumeyrolle[1], Jenni S. S. Kontkanen[2,3], Clémence Rose[4], Alejandra Velazquez Garcia[1,5], Eric Bourrianne[1], Maxime Catalfamo[1], Véronique Riffault[5], Emmanuel Tison[5], Joel Ferreira de Brito[5], Nicolas Visez[6], Nicolas Ferlay[1], Frédérique Auriol[1], and Isabelle Chiapello[1]

[1]UMR 8518 Laboratoire d'Optique Atmosphérique (LOA), CNRS, Université de Lille, 59000 Lille, France
[2]CSC – IT Center for Science, 02101 Espoo, Finland
[3]Institute for Atmospheric and Earth system Research, University of Helsinki, 00014 Helsinki, Finland
[4]Laboratoire de Météorologie Physique, LaMP-UMR 6016, CNRS, Université Clermont Auvergne, 63178 Aubière, France
[5]IMT Nord Europe, Institut Mines-Télécom, Centre for Energy and Environment, Université de Lille, 59000 Lille, France
[6]UMR 8516 – LASIRE – LAboratoire de Spectroscopie pour les Interactions, la Réactivité et l'Environnement, CNRS, Université de Lille, 59000 Lille, France

Correspondence: Suzanne Crumeyrolle (suzanne.crumeyrolle@univ-lille.fr)

Received: 24 June 2022 – Discussion started: 20 July 2022
Revised: 17 November 2022 – Accepted: 27 November 2022 – Published: 5 January 2023

Abstract. Formation of ultrafine particles (UFPs) in the urban atmosphere is expected to be less favored than in the rural atmosphere due to the high existing particle surface area acting as a sink for newly formed particles. Despite large condensation sink (CS) values, previous comparative studies between rural and urban sites reported higher frequency of new particle formation (NPF) events over urban sites in comparison to background sites as well as higher particle formation and growth rates attributed to the higher concentration of condensable species. The present study aims at a better understanding the environmental factors favoring, or disfavoring, atmospheric NPF over Lille, a large city in the north of France, and to analyze their impact on particle number concentration using a 4-year long-term dataset.

The results highlight a strong seasonal variation of NPF occurrences with a maximum frequency observed during spring (27 events) and summer (53 events). It was found that high temperature ($T > 295$ K), low relative humidity (RH < 45 %), and high solar radiation are ideal to observe NPF events over Lille. Relatively high CS values (i.e., $\sim 2 \times 10^{-2}$ s^{-1}) are reported during event days suggesting that high CS does not inhibit the occurrence of NPF over the ATmospheric Observations in LiLLE (ATOLL) station. Moreover, the particle growth rate was positively correlated with temperatures most probably due to higher emission of precursors. Finally, the nucleation strength factor (NSF) was calculated to highlight the impact of those NPF events on particle number concentrations. NSF reached a maximum of four in summer, evidencing a huge contribution of NPF events to particle number concentration at this time of the year.

Published by Copernicus Publications on behalf of the European Geosciences Union.

1 Introduction

New particle formation (NPF) leads to the formation of a large number of particles with diameters below 20 nm that will contribute significantly to the high levels of fine particles observed in ambient air. These particles can have adverse effect on human health as they can penetrate deeply into the pulmonary system (Clifford et al., 2018; Ohlwein et al., 2019). The freshly formed particles then grow to larger sizes ($D_p > 100$ nm) at which they may act as cloud condensation nuclei (CCN, Pierce and Adams, 2009; Ren et al., 2021; Rose et al., 2017; Spracklen et al., 2006). NPF events have been observed around the world (Kerminen et al., 2018; Kontkanen et al., 2017; Kulmala et al., 2004) in various environments from the boundary layer at urban locations (Kanawade et al., 2022; Roig Rodelas et al., 2019; Tuch et al., 2006; Wehner and Wiedensohler, 2003) as well as remote polar background areas (Dall'Osto et al., 2018) but also within the free troposphere (Rose et al., 2015a, b). NPF events are typically associated with a photochemical origin, thus occurring mostly during daytime (Kulmala et al., 2014), with some scarce events being observed during nighttime (Roig Rodelas et al., 2019; Salimi et al., 2017).

NPF occurrence depends on various factors including precursor emission strength, number concentration of pre-existing aerosol population, meteorological parameters (in particular solar radiation, temperature, and relative humidity, RH), and the oxidation capacity of the atmosphere (Kerminen et al., 2018). Differences were found in both the seasonality and intensity of NPF events according to the site type (urban, traffic, regional background, rural, polar, and high altitude; Dall'Osto et al., 2018; Sellegri et al., 2019). This variability seems to be related to environmental conditions specific to each location, which makes it hard to draw general conclusions on the conditions that trigger NPF events (Berland et al., 2017; Bousiotis et al., 2021). However, Nieminen et al. (2018) highlighted a common seasonal occurrence of NPF during spring and summer using datasets from 36 continental sites worldwide.

The formation and growth of initial clusters to detectable sizes ($D_p > 1$–3 nm) compete with their simultaneous removal from the ultrafine particle (UFP) mode by coagulation with pre-existing particles (Kerminen et al., 2001; Kulmala, 2003). For that reason, the number concentration of particles smaller than 20 nm has been observed to be anti-correlated with the aerosol volume and mass concentration over a rural area in northern Italy (Rodríguez et al., 2005). Indeed, the total aerosol volume is rather small during NPF events (Kerminen et al., 2018; Rodríguez et al., 2008). While the negative effect of increased pre-existing particle surface area (often described with the condensation sink, CS) on the occurrence of these events is widely accepted (Kalkavouras et al., 2017), yet cases are found when NPF events occur on days with higher CS compared to average conditions (Größ et al., 2018; Kulmala et al., 2017).

A recent study by Bousiotis et al. (2021) used large datasets (16 sites) over Europe (6 countries) and highlighted that solar radiation intensity, temperature, and atmospheric pressure had a positive relationship with the occurrence of NPF events at the majority of sites (exceptions were found for the southern sites), either promoting particle formation or increasing the growth rate (GR). Indeed, solar radiation is considered one of the most important factors in the occurrence of NPF events, as it contributes to the production of NPF precursors (Kontkanen et al., 2016). Higher temperatures are considered favorable for the growth of newly formed particles (Dada et al., 2017), as they can be linked to higher concentrations of organic vapor (Wang et al., 2013) that support particulate growth but also reduce the stability of the initial molecular clusters (Deng et al., 2020; Kurtén et al., 2007).

Wind speed, on the other hand, has shown variable effects on the occurrence of NPF events, appearing to depend on the site location rather than their type (Bousiotis et al., 2021). Additionally, the origin of the incoming air masses plays a very important role, since air masses of different origins have different meteorological, physical, and chemical characteristics. Therefore, the probability of NPF event occurrence at a given location and time depends not only on local emissions but also on long range transport (Sogacheva et al., 2007, 2005; Tunved et al., 2006) and on synoptic meteorological conditions at the European scale (Berland et al., 2017).

Formation of new particles in the urban atmosphere is expected to be less favored than in the rural atmosphere due to the high existing surface area of particles acting as a sink for freshly formed particles. Despite the large CS values, previous comparative studies between rural and urban sites reported a higher frequency of NPF events over urban sites in comparison to background sites (Peng et al., 2017), where higher particle formation and higher GR (Nieminen et al., 2018; Salma et al., 2016; Wang et al., 2017) were also observed and attributed to the higher concentration of condensable species. This study presents the first observations of NPF events over Lille, a large city in the north of France. Based on a multi-annual dataset (2017–2020), the frequency and intensity of the NPF events are analyzed, aiming at better defining the favorable and unfavorable conditions.

2 Materials and methods

The ATmospheric Observations in LiLLE (ATOLL, Fig. 1) station is located in Villeneuve-d'Ascq, northern France (50.6114° N, 3.1406° E, 60 m a.s.l.), only 6 km away from the city center of Lille, which is the core of the metropolis (Métropole Européenne de Lille, with more than 1.1 million inhabitants) to which Villeneuve-d'Ascq belongs. Low single scattering albedo (SSA) values (0.75 on average within the PM_1 fraction; Velazquez-Garcia et al., 2022) and large particle number concentrations (6140 cm^{-3} on average) suggest

that aerosol measurements performed at ATOLL are comparable to global atmospheric watch (GAW) sites classified as urban (Laj et al., 2020; Rose et al., 2021). ATOLL is also part of the Aerosols, Clouds, and Trace gases Research InfraStructure (ACTRIS, http://www.actris.net, last access: 1 October 2022), providing high-quality long-term atmospheric data in northern France. This station is under the influence of many anthropogenic sources, e.g., road traffic, residential sector, agriculture, and industries (Chen et al., 2022), as well as maritime emissions, and is episodically under the influence of natural events such as aged volcanic plumes and Saharan dust (Boichu et al., 2019; Bovchaliuk et al., 2016; Mortier et al., 2013).

A large set of in situ and remote sensing instruments are implemented at ATOLL to characterize physical, chemical, optical, and radiative properties of particles and clouds. In situ instruments have independent sampling stainless steel lines located at least 1 m above the roof top and equipped either with PM_1 cyclone or PM_{10} inlet. The measurements used for the present study were performed between 1 July 2017 and 31 December 2020 with the instruments that are described below.

The scanning mobility particle sizer (SMPS) measures every 5 min the particle number size distribution between 15.7 and 800 nm (divided in more than 100 bins) downstream of a Nafion membrane as recommended by ACTRIS standards to keep RH below 40 %. The SMPS system consisted of a condensation particle counter (TSI model 3775), differential mobility analyzer (DMA, TSI 3081A) as described by Villani et al. (2007), and a nickel aerosol neutralizer (Ni-63 95MBq). The sheath flow rate was controlled with a critical orifice in a closed loop arrangement (Jokinen and Mäkelä, 1997). The scan time was 300 s and the particle concentrations were corrected by taking into account charge effects and diffusion calculated using the manufacturer software and algorithms (AIM 10.2.0.11).

Accordingly, aerosol number size distribution data from the SMPS measurements were used to classify individual days as NPF event, undefined, or non-event days. The classification procedure, presented in Dal Maso et al. (2005), follows the decision criteria based on the presence of UFP ($D_p < 25$ nm) and their subsequent growth to Aitken mode ($D_p < 80$ nm). Briefly, event days are identified when sub-25 nm particle formation and growth are observed. Undefined days correspond to days when sub-25 nm particle formation is observed for more than 1 h, but those particles are not growing so their diameter remains below 25 nm. On non-event days the nucleation mode is absent.

SMPS particle number size distributions were also used for CS (Eq. 1) and GR (Eq. 3) calculations. The CS estimates the loss rate of the condensable vapors (Kulmala et al., 2001), which were assumed to have molecular properties similar to sulfuric acid for CS calculation (Dal Maso et al., 2005):

$$\mathrm{CS} = 2\pi D \sum_i \beta_{Mi} D_{p,i} N_i \,, \tag{1}$$

where D is the diffusion coefficient of the condensing vapor; $D_{\mathrm{p,i}}$ and N_i the particle diameter and number concentration for size bin i, respectively; and β_{Mi} the transitional correction factor (Fuks and Sutugin, 1970) defined in Eq. (2):

$$\beta_{Mi} = \frac{1+Kn}{1+0.337Kn+\frac{4}{3}\alpha^{-1}Kn+\frac{4}{3}\alpha^{-1}Kn^2}, \tag{2}$$

with Kn the Knudsen number, and α the accommodation coefficient (here, set to unity).

A high CS indicates the presence of a large particulate surface area onto which NPF precursors can condensate.

The particle GR from 15.7 to 30 nm ($\mathrm{GR}_{15.7\text{–}30\,\mathrm{nm}}$) was calculated based on the maximum-concentration method described in Kulmala et al. (2012). For each event, the NPF starting time (T_1) was first identified when the newly formed mode was observable in the first bin of the SMPS ($D_{\mathrm{p},1} = 15.7$ nm). Then, the time (T_2) when the number concentration of particles with diameter ($D_{\mathrm{p},2}$) of 30 nm (N_{30}) peaked was also manually identified. Particle $\mathrm{GR}_{15.7\text{–}30\,\mathrm{nm}}$ was then calculated by linear regression of particle size vs. time span from the NPF start until the time when N_{30} reaches a maximum:

$$\mathrm{GR}_{15.7\text{–}30\,\mathrm{nm}} = \left(D_{\mathrm{p},2} - D_{\mathrm{p},1}\right)/\left(T_2 - T_1\right). \tag{3}$$

An aerosol chemical speciation monitor (ACSM, Aerodyne Research Inc.) equipped with a $PM_{2.5}$ cut-off inlet (URG Cyclone 2000-30EH, Chapel Hill, NC, USA) and with a primary flow of 3 L min^{-1} was used to monitor the aerosol chemical composition at ATOLL. The chemical characterization of non-refractory submicron particles ($\mathrm{NR\text{-}PM}_1$), that is to say material vaporizing around 600 °C under close-to-vacuum conditions, was performed online and in real time every 30 min. This instrument is based on the same principle as the aerosol mass spectrometers (AMS), without providing aerosol size distribution information. A full description of the instrument is available in Rivellini et al. (2017). Under ambient conditions, mass concentrations of particulate organics, sulfate, nitrate, ammonium, and chloride are obtained with a detection limit $< 0.2\,\mu\mathrm{g\,m^{-3}}$ for 30 min of signal averaging. An algorithm (Middlebrook et al., 2012) was applied to ACSM mass concentrations to obtain a time-dependent correction of the collection efficiency ranging from 0.45 to 0.83.

Absorption coefficients (σ_{abs}) were continuously measured with a 7-wavelength aethalometer (AE33, Magee Scientific Inc., Cuesta-Mosquera et al., 2021). According to ACTRIS current guidelines (https://actris-ecac.eu/particle-light-absorption.html, last access: 1 October 2022), σ_{abs} coefficients at each wavelength have been recalculated by (1) multiplying equivalent black carbon (eBC) by the mass-specific absorption coefficient (MAC) and then (2) dividing by the suitable harmonization factor to account for the filter multiple scattering effect, i.e., 2.21 (M8020 filter tape) in 2017 and 1.76 (M8060 filter tape) afterwards. The aethalometer samples at 5 L min^{-1} downstream of a PM_1 cyclone (BGI SCC1.197, Mesa Labs). The spectral dependency

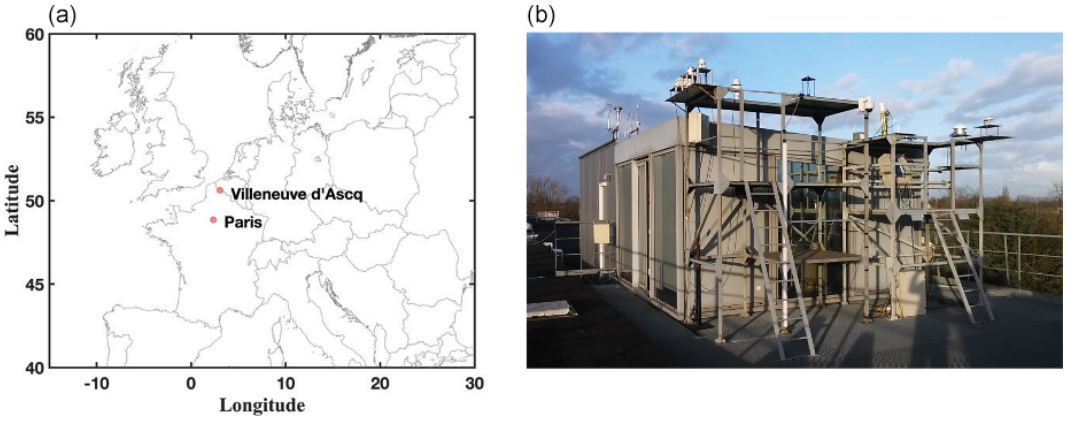

Figure 1. ATOLL location in Villeneuve-d'Ascq (northern France), and a picture of the station on the rooftop of the University of Lille P5 building (© LOA).

of σ_{abs} was used to determine the contributions of traffic (fossil fuel – BC_{ff}) and wood burning (BC_{wb}) to eBC via a source apportionment model (Sandradewi et al., 2008).

Meteorological data including temperature and water vapor mixing ratio were also measured every minute at the sampling site using a weather station (DAVIS Inc weather station, Vantage Pro 2). Solar radiation at the surface was measured every minute at the sampling site using a set of Kipp & Zonen pyranometers (CM22, for diffuse fluxes using a sphere shadower) and normal incidence pyrheliometer (CH1 for direct fluxes), with the solar radiation being then calculated as the sum of the diffuse and direct fluxes. The cloud cover was estimated from the Findclouds algorithm, provided by the manufacturer, and applied on sky imager (Cloudcam, CMS) pictures by comparing the different values of the red, green, and blue components of each pixel of the image taken (Shukla et al., 2016).

Three-day air mass back trajectories of the air masses arriving at ATOLL at half the boundary layer height between 1 July 2017 and 31 December 2020 were computed every hour using the hybrid single-particle Lagrangian integrated trajectory (HYSPLIT version 5.1.0) transport and dispersion model from the NOAA Air Resources Laboratory (Rolph et al., 2017; Stein et al., 2015) and meteorological input from the global data assimilation system (GDAS) at $1 \times 1°$ resolution, resulting in 30 719 back trajectories.

3 Results

3.1 NPF event frequency

The seasonal distribution of NPF events at ATOLL is displayed in Fig. 2. SMPS missing data (in Fig. 2) reach up to about 40 % from January to April due to the yearly calibrations at the manufacturer premises and a few laboratory campaigns (October 2018–June 2019). Over the 4 years of measurements (2017–2020), 96 d (11 %) were classified as NPF event days (Ev), 355 (40 %) as undefined days (Un) and 432 (49 %) as non-event days (No). One can also note that most of the NPF events identified were observed during spring (March–April–May, with 27 events corresponding to 15 % of days when observations were available during this season over the 4-year period) and summer (June–July–August, with 53 events corresponding to 19 %), with a maximum observed in June consistent with a previous study over central Europe (Dall'Osto et al., 2018). During winter, the number of events is extremely limited (only one event observed in February). In the following sections, only observations from spring and summer seasons will be discussed due to the low representativeness of NPF events in fall ($n = 15$) and winter ($n = 1$). Moreover, the undefined event days are seen all year round (frequency around or larger than 20 %) with a clear peak in August (frequency at 62 %) consistent with observations over the boreal forest where undefined days were also observed to be most frequent in early fall (Buenrostro Mazon et al., 2009).

Using long-term measurements from 36 sites (polar, rural, high altitude, remote, and urban), Nieminen et al. (2018) reported an annual NPF frequency below 15 % for half of the sites (18 sites from all types) and occasionally over 30 % for 10 sites. Moreover, they highlighted a seasonal variation of NPF occurrence with larger (lower) frequency, about 30 % (10 %), during spring (winter). A frequency analysis of NPF occurring only over urban or anthropogenically influenced sites show large site-to-site differences for all seasons. Indeed, Nieminen et al. (2018) reported NPF occurrence frequencies varying from 20 % (Helsinki, Finland; Sao Paulo, Brazil) to 80 % (Beijing, China; Marikana, South Africa) during spring and from 7 % (Helsinki) to 78 % (Marikana) during winter. Yearly averages of NPF occurrence frequencies are between 11 % (Helsinki) and more than 60 % (Beijing and Marikana).

The ATOLL event frequency (seasonal variation and values) is similar to observations performed in Paris while the

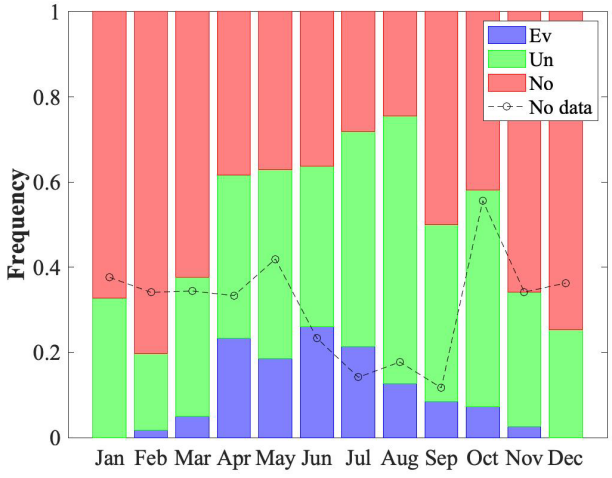

Figure 2. Seasonal distribution of event days (Ev, blue), undefined days (Un, green), and non-event (No, red) days at the ATOLL station, Lille, France, during 2017–2020. Days with missing data are excluded from the total number of days per month and the frequency of missing data are indicated with the black circles.

frequency of undefined and non-event days is quite different (Dos Santos et al., 2015). Indeed, in Paris the non-event frequency is larger than 60 % except in July and August, whereas over ATOLL the non-event frequency shows a clear seasonal pattern with lower frequency (< 40 %) from April to August. Moreover, undefined event frequency in Paris shows a minimum (< 5 %) in May and June and remains quite steady during the rest of the year (around 20 %). One can note that the frequency of undefined events is much higher over ATOLL all year long with an average of 40 %. The frequency of undefined events observed at ATOLL is clearly larger than the frequencies observed over a more polluted site (Paris) and similar to those observed over pristine sites in Siberian and Finnish boreal forests (Uusitalo et al., 2021). This could mean that ATOLL is under the influence of air masses or particle and precursor sinks that favor the burst of UFP.

3.2 Aerosol number size distribution

Hourly averaged median particle number size distributions (PNSDs) obtained from the SMPS are shown in Fig. 3 separately for NPF event (around 800 PNSD), undefined (around 2300 PNSD), and non-event (around 1700 PNSD) days observed during the warm period (only spring and summer). For all event days, the PNSD were first sorted for each hour of the day. Then, the median PNSD was calculated for each hour of the day. PNSD shown in Fig. 3a is then representative of a "typical" NPF event day (Kulmala et al., 2022). The same data filtering was done for PNSD observed during undefined (Fig. 3b) and non-event days (Fig. 3c). Atmospheric NPF and subsequent particle growth are seen in Fig. 3a as an appearance of new aerosol particles with small diameters followed by the growth of these particles toward larger sizes. If this phenomenon is taking place regionally (few tens of km in radius), a so called "banana plot" is observed in PNSD as a function of time at a fixed location. The time evolution of the PNSD for "typical" NPF event day (Fig. 3a) displays a similar growth pattern for newly formed particles to the one observed for individual NPF event days (see Figs. S1 and S2 in the Supplement for examples). Indeed, one can clearly see a UFP mode appearing from 10:00 to 15:00 (UTC) and growing during the rest of the day. The NPF starting time and the growth rate will be discussed in the following section. By 23:00 UTC, the newly formed particles reach an average diameter of 50 nm, similar to the median modal diameter of the pre-existing particles observed during the morning (00:00–08:00 UTC). The PNSD observed during "typical" undefined days (Fig. 3b) highlights a burst of UFP again from 10:00 to 15:00 UTC that neither grow nor persist over the whole afternoon. The behavior of the median PNSD is again similar to the individual undefined events observed during this period (not shown here). The PNSD observed during "typical" non-event days (Fig. 3c) shows no sign of particle growth, as expected.

3.3 NPF starting time and growth rate

Figure 4 shows the monthly variation of the starting time and particle $GR_{15.7–30\,nm}$ of each event observed at ATOLL. Most NPF events start between 09:00 and 14:00 UTC (74 %), with fewer events starting in the early morning (07:30–09:00 UTC, 6 %) and late afternoon (15:00 and 19:30 UTC, 20 %). NPF starting time as well as $GR_{15.7–30\,nm}$ strongly depend on the month during which the event is observed. Indeed, the NPF starting time occurs later during spring days on average (also true for fall and winter), while the earliest time was reached in May and June (around 08:20 UTC). Nocturnal events are rarely observed, with only one occurrence in August 2018. No diurnal NPF event was observed after 16:00 UTC in summer. During spring and fall, the average NPF starting time varies between 10:00 and 19:00 UTC. The start time monthly variability seems linked to sunrise and sunset times. In the following section, the relationship between the total solar irradiation and NPF occurrence will be examined.

The event ending time was determined as the time when the growth of the freshly formed particles was over, i.e., when the diameter reached the diameter of the pre-existing particles. The duration of the nucleation events at ATOLL was then estimated and varies from 1 h up to 28 h. On average, NPF duration is shorter from May to August (around 8 h) and increases up to around 13 h on average in March. This seasonal behavior could be due to the presence or availability of condensable vapors, air mass origins, and environmental conditions favorable to NPF events (see Sect. 3.2).

The $GR_{15.7–30\,nm}$ values observed at ATOLL lie within 0.8 to 15.7 $nm\,h^{-1}$ and show a strong monthly variability with

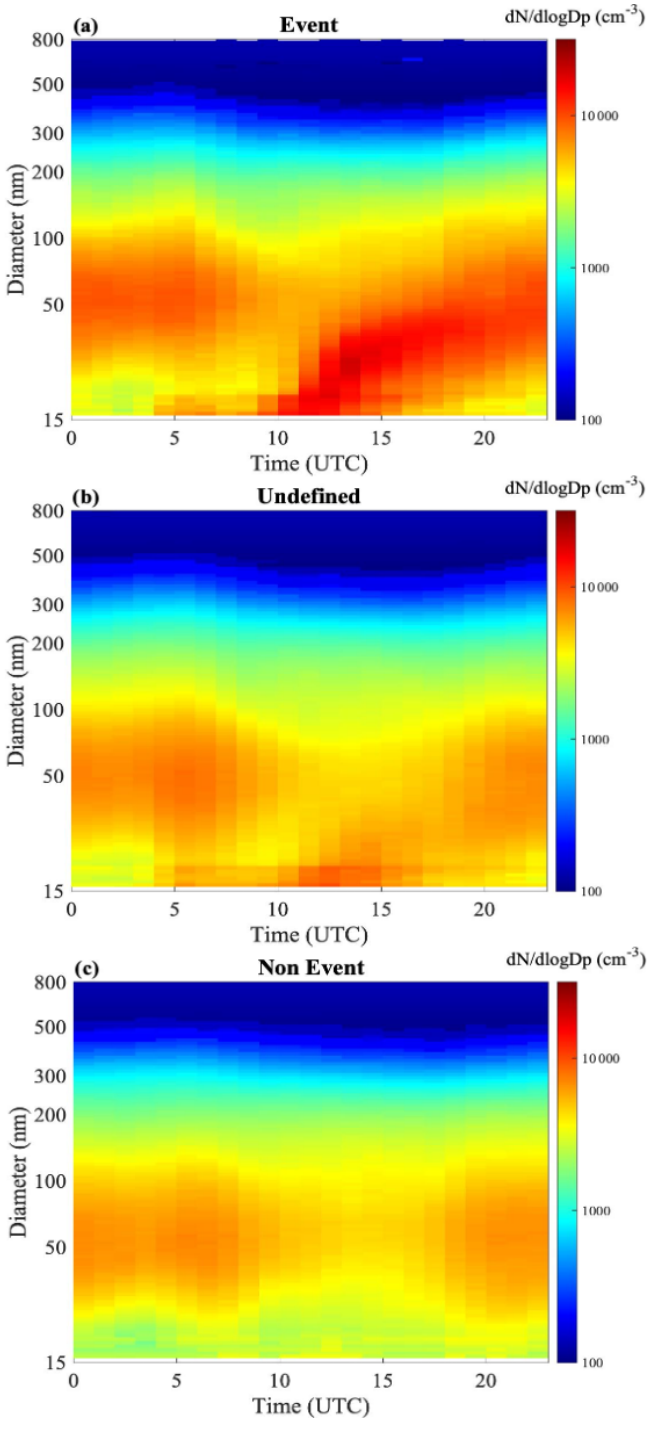

Figure 3. Hourly median particle number size distribution ($15.7\,\text{nm} < D_p < 800\,\text{nm}$) observed during NPF event **(a)**, undefined **(b)**, and non-event **(c)** days in spring and summer from 2017 to 2020.

the lowest values observed in spring (and fall, not shown here). The largest median values are observed in May and August, while the 75th percentile highlights larger values of $GR_{15.7–30\,nm}$ during summer (Fig. 4b). $GR_{15.7–30\,nm}$ values were in addition plotted as a function of temperature for all years and seasons in Fig. 5, which highlights that below 20 °C, $GR_{15.7–30\,nm}$ values are lower than $6\,\text{nm}\,\text{h}^{-1}$, while, under warmer conditions ($T > 20\,°\text{C}$), $GR_{15.7–30\,nm}$ reach values up to $16\,\text{nm}\,\text{h}^{-1}$. These results show a temperature dependence ($R \approx 0.4$) of the particle growth consistent with previous observations over the boreal forest (Liao et al., 2014). Higher temperatures have been shown to favor the emission of biogenic precursors, including monoterpenes known to favor the occurrence of NPF events (Kulmala et al., 2004). Previous studies (Paasonen et al., 2018; Yli-Juuti et al., 2011) have shown that GRs usually exhibit larger values during warm periods especially during summer, and that there is a link between GR seasonal patterns and the high abundance of biogenic volatile organic compounds (VOCs) during warmer periods (spring and summer) over the boreal forest. Therefore, the observed seasonal variation of $GR_{15.7–30\,nm}$ may be related to temperature-dependent emissions of organic compounds in the vicinity of ATOLL (Fig. 5). This hypothesis is supported by the larger contribution of organics during NPF event days observed in Fig. 9. However, over urban areas such as Beijing or Shanghai, $GR_{15–25\,nm}$ showed no clear seasonal variation (Yao et al., 2018). As previously observed in Fig. 3a, the median diameter reached at the end of all NPF events is around 50 nm. Moreover, the seasonal variation of the NPF event durations could be related to the $GR_{15.7–30\,nm}$ seasonal variation. The lower $GR_{15.7–30\,nm}$ values are associated with the longer NPF duration. The seasonal variation of NPF duration highlighted earlier could then only be a consequence of the $GR_{15.7–30\,nm}$ seasonal variation.

3.4 Environmental conditions

The cloud fraction was calculated from the sky imager dataset following the method by Shukla et al. (2016) and sorted as a function of event, undefined, and non-event days. The effect of cloudiness on NPF event occurrence is shown in Fig. 6a, with a specific focus on measurements collected between 09:00 and 14:00 UTC, i.e., the period of time where most NPF events tended to start. There is a clear inverse correlation between cloud fraction and NPF occurrences. The average cloud fraction is around 0.47 during event days, 0.68 during undefined days, and 0.74 during non-event days. Moreover, the 25th percentiles of the cloud fractions for NPF event (0.06), undefined (0.47), and non-event days (0.63) clearly show that the absence of clouds (lower cloud fraction) is mostly associated with NPF event days. This result is consistent with previous studies performed over the boreal forest (Dada et al., 2017) and is linked to the fact that radiation seems essential for NPF during the warmer period (spring and summer), as the events occur almost solely during daylight hours (Kulmala et al., 2004). Figure 6b shows the average diel total solar radiation observed during NPF event, non-event, and undefined days for spring and summer.

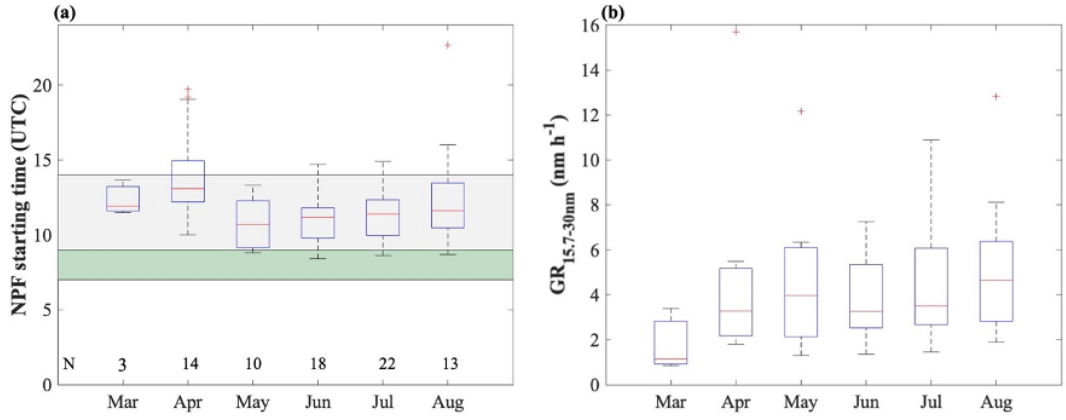

Figure 4. Monthly variation of NPF events **(a)** starting time and **(b)** their growth rate ($GR_{15.7–30\,nm}$) at the ATOLL station during 2017–2020. The boxes and whiskers (bottom to top) represent the 10th and 25th percentiles, median (red line), and the 75th and 90th percentiles. Crosses represent the outliers. The grey area represents the period, from 09:00–14:00 UTC, when most of the NPF events occur. The blue area corresponds to the period before the NPF onset (07:00–09:00 UTC). N represents the number of events observed per month.

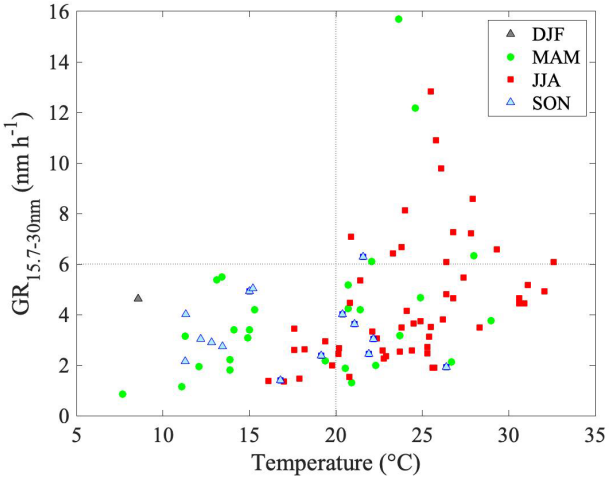

Figure 5. Growth rate ($GR_{15.7–30\,nm}$) values as a function of ambient temperature for different seasons.

As expected, the total solar radiation is on average always larger during event days in comparison to non-event days, with a more pronounced difference observed during spring.

Other environmental parameters known to influence the occurrence of NPF events, such as temperature and RH, were also investigated to highlight diel and seasonal variations (Fig. 7). Our results confirm that NPF is favored by low values of ambient RH (Fig. 7a), especially during spring, consistent with previous studies (Duplissy et al., 2016; Hamed et al., 2011; Merikanto et al., 2016). A few reasons can explain this tendency: (1) high RH values (RH > 90 %) observed at the surface are usually associated with the presence of low-altitude clouds reducing the incoming total radiation and then preventing NPF occurrence; (2) at moderately high RH (RH > 40 %), hydrophilic aerosols could grow through condensation which will enlarge the sink for possible precursors; and (3) high RH values may limit the formation of some semi-volatile VOCs through ozonolysis reactions, inhibiting the formation of condensable vapors necessary for nucleation (Fick et al., 2003; Tillmann et al., 2010).

Figure 7b shows the diel median temperature conditions (T) during NPF event, non-event, and undefined days. NPF events occurred for temperatures ranging between 3 and 33.5 °C. In both seasons, averaged temperatures during event days are always larger than during non-event days, again with larger differences during spring. One should note that days with high temperatures in spring and summer are usually also days with high solar radiation, consistent with conclusions from Fig. 6. The temperature difference between undefined days and event days is clearly marked during spring and fades away during summer. As previously discussed, higher temperatures favor the emission of biogenic precursors, including monoterpenes, known to favor the occurrence of NPF events (Kulmala et al., 2004). Isoprene emission is also larger at higher temperatures, but according to Heinritzi et al. (2020) it is one example where a biogenic compound inhibits NPF events. Moreover, a high temperature can also lead to the evaporation of molecular clusters which may inhibit NPF events (Dada et al., 2017; Deng et al., 2020).

3.5 Condensation sink

The CS characterizes the loss rate of atmospheric vapors to aerosol particles. The diel variations of CS calculated for spring and summer for NPF event, undefined, and non-event days are shown in Fig. 8a. Hourly averaged CS values are high (larger than $2 \times 10^{-2}\,s^{-1}$) during NPF event days occurring during spring and summer (Fig. 8a). CS values ranging from 0.6 up to $10.7 \times 10^{-2}\,s^{-1}$ were reported during NPF event days and over different urban sites (Beijing, Nanjing

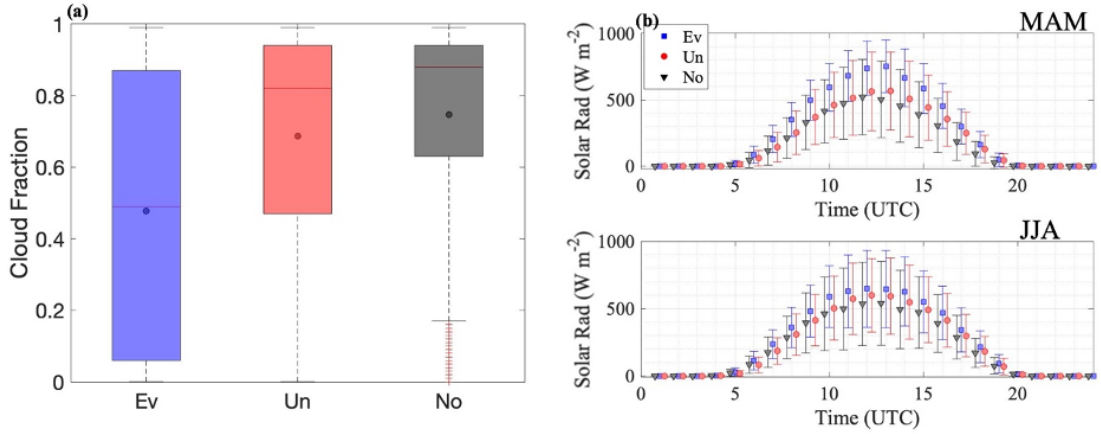

Figure 6. **(a)** Cloud fraction observed from 09:00 to 14:00 UTC during event (Ev), undefined (Un), and non-event (No) days. The red line represents the median and the circles the average, while the lower and upper edges of the box represent the 25th and 75th percentiles, respectively. The lower and upper edges of the whisker correspond to the 10th and 90th percentiles, respectively. **(b)** Diel variations (UTC) of the mean total solar radiation observed during the event days (Ev, blue squares), undefined days (Un, red dots), and non-event days (No, black triangles) during spring (MAM, top) and summer (JJA, bottom) seasons **(b)**. The error bars correspond to one standard deviation.

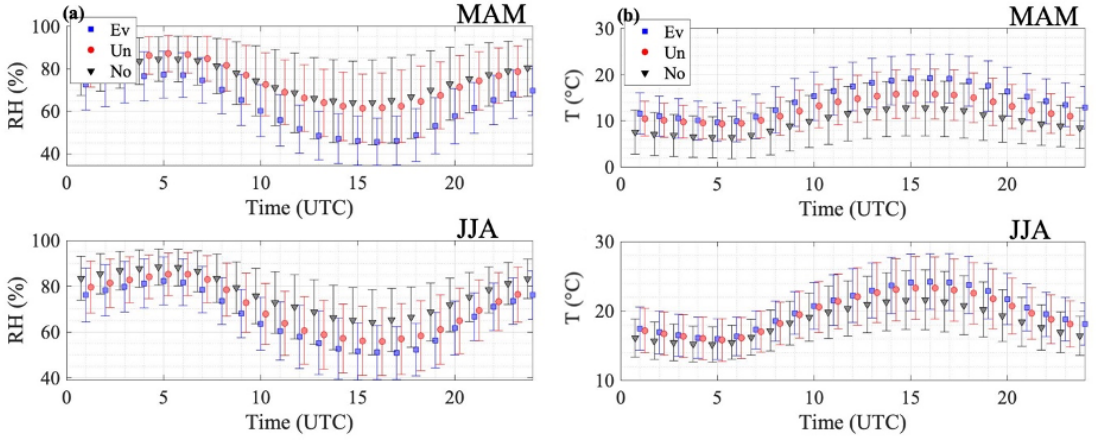

Figure 7. Diel variations (UTC) of the mean relative humidity (RH, **a**) and mean temperature **(b)** observed during the NPF event days (Ev, blue squares), undefined days (Un, red dots), and non-event days (No, black triangles) during spring (MAM) and summer (JJA) seasons. The error bars correspond to one standard deviation.

or Hong Kong) (Xiao et al., 2015). Over pristine sites, such as Hyytiälä (Finland), the CS values are between 0.05 and 0.35×10^{-2} s^{-1}. Low values of CS, often considered as the major limiting factor in the NPF occurrence, do not inhibit the occurrence of NPF events at ATOLL, consistent with previous observations in similar environments, such as the Melpitz (Germany) observatory (Größ et al., 2018) or over Chinese megacities (Xiao et al., 2015). One can assume that the presence of large concentrations of precursors could explain the formation of particles over polluted sites such as ATOLL. Unfortunately, precursors were not measured over the 4-year period; therefore, this assumption would require further investigation beyond the scope of this study. Nevertheless, recent studies, performed in the CLOUD chamber, demonstrate that the presence of nitric acid (HNO_3) and ammonia (NH_3), typical within urban environments and particularly in the north of France (Roig Rodelas et al., 2019), contribute to fresh particle survival by dramatically increasing their growth rate (Marten et al., 2022; Wang et al., 2020).

In the afternoon of NPF event days, the CS increases due to the growth of freshly emitted particles, especially during summer. The contribution of newly formed particles ($D_p <$ 50 nm) to the CS is about 36 % and 27 % during summer and spring, respectively, while the contribution of pre-existing particles ($D_p >$ 150 nm) to the CS is below 20 % for both seasons. Moreover, during non-event days the size-resolved median CS is shifted toward larger particle diameters with a maximum observed around 100 nm for all seasons.

To evaluate the impact of the background CS on NPF occurrences, all CS values observed from 07:00–09:00 UTC

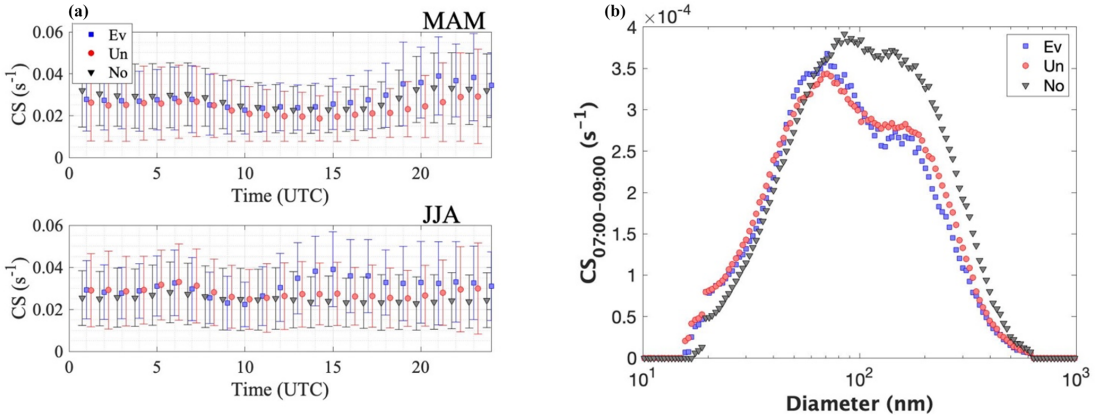

Figure 8. **(a)** Diel variations of the condensation sink (CS) during spring (MAM) and summer (JJA) seasons, and **(b)** median size-resolved background CS (from 07:00 to 09:00 UTC) for MAM and JJA during event days (Ev, blue squares), undefined (Un, red dots), and non-event days (No, black triangles).

($CS_{07:00–09:00}$), the period before the NPF starting time (green area on Fig. 4a), were averaged during NPF event, non-event, and undefined days. It was found that the total $CS_{07:00–09:00}$ was larger (around 16 %) during non-event days in comparison to undefined and event days. Moreover, this difference is mostly due to particles larger than 70 nm according to the size-resolved $CS_{07:00–09:00}$ (Fig. 8b). The difference between non-event and event days is lower than what is usually observed over pristine sites (Lyubovtseva et al., 2005) but significant enough to trigger the NPF event occurrence.

Du et al. (2022) studied the chemical composition of particles contributing to the CS when NPF occurrence is at its highest (10:00–15:00 local time) over Beijing. They observed a large increase of nitrate and a decrease of organics in $PM_{2.5}$ with increasing CS values for NPF event and non-event days. As the CS observed over ATOLL is largely influenced by the freshly formed particles, the chemical composition of particles as a function of CS can be presented during two specific periods: before (07:00–09:00 UTC) and during (09:00–14:00 UTC) the period when the NPF occurrence is at its highest for NPF event and non-event days (Fig. 9). During non-event days, both periods (Fig. 9b and d) exhibit a similar mass fraction for all compounds with on average 41 % of organics, 16 % of nitrate, 21 % of sulfate, 11 % of ammonium, less than 1 % of chloride, and around 10 % of black carbon (BC). As the aerosol sources during non-event days are supposed to be the same throughout the day, this result was actually expected.

Larger contribution of organics to the CS is observed for NPF event days during the NPF period ($CS_{09:00–14:00} \sim 54$ % on average, Fig. 9c) in comparison with the period right before the start of the NPF events ($CS_{07:00–09:00} \sim 46$ % on average, Fig. 9a). Indeed, for large values of $CS_{09:00–14:00}$ ($> 0.045\ s^{-1}$) the contribution of organics is larger than 50 %, reaching a maximum of 69 % for $CS_{09:00–14:00}$ of $0.085\ s^{-1}$. This result suggests that organic vapors may be involved in the particle growth.

Additionally, the correlation coefficients (R) between meteorological parameters and gaseous or particulate pollutants are reported in Table 1 for the entire period of measurements (all seasons). Hourly averages over a time window between 09:00 and 14:00 UTC (NPF event starting time period) of a few variables (total CS, T, RH, and BC from wood burning (BC_{wb})) were used to calculate those correlation coefficients (corresponding to 7025 and 35 433 data points for NPF event and non-event days, respectively).

The correlation of BC_{wb} with the CS during non-event days is high ($R = 0.67$) and is clearly absent during NPF event days ($R = 0.19$). One can also note that NO_x concentrations have a positive correlation (0.30) with CS during NPF non-event days, while the same correlation is negative (−0.17) during NPF event days. NO_x sources over urban areas are mostly anthropogenic ones (residential heating, traffic, and industries), which is consistent with its relatively high correlation coefficients with BC_{wb} (0.47 and 0.65). As highlighted in Barreira et al. (2021), BC_{wb} and NO_x are evolving through the year showing a minimum in summer and a maximum in winter when sources are stronger due to colder temperatures and residential heating emissions. As non-event days are mostly (62 %) observed during cold months (fall and winter, not shown here) and NPF events are largely (82 %) observed during warmer months (spring and summer), the correlation between BC_{wb}, NO_x, and CS during non-event days is expected. However, during spring, air masses observed during NPF events are clearly "cleaner" (in terms of NO_x and BC_{wb}) than non-event cases. Indeed, NO_x and BC_{wb} concentrations are lowered by 18 % and 36 %, respectively, during NPF event days occurring in spring in comparison to non-event days. During summer, NO_x and BC_{wb} concentrations reach an annual minimum, and therefore both pollutant concentrations are similarly correlated be-

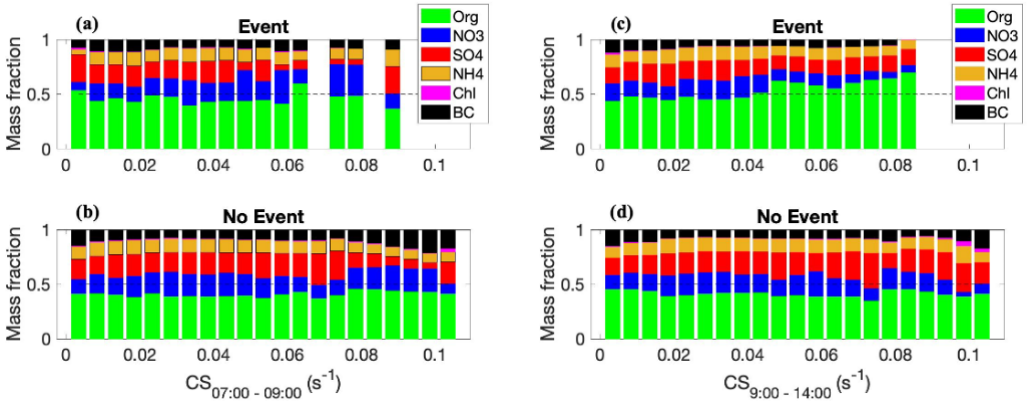

Figure 9. Mass fractions of the major compound measured before (07:00–09:00 UTC, **a, b**) and during (09:00–14:00 UTC, **c, d**) the NPF period at the ATOLL station during event **(a, c)** and non-event **(b, d)** days. The black dashed line corresponds to 50 % mass fraction.

tween NPF event and non-event days (lowered by −0.04 % and 0.01 % during NPF event days).

Moreover, during NPF event days the temperature is positively correlated (0.55) with the CS, while during non-event days this correlation is clearly not observed (0.06). As discussed previously, this coupling was expected as it could be related to larger VOC emissions leading to enhanced particle growth and to higher concentrations of larger particles (Sect. 3.4).

3.6 Air mass trajectories

Environmental parameters such as CS, T, and RH (Figs. 6, 7 and 8) observed during undefined events exhibit values mostly between those observed during event and non-event days. A deeper analysis of undefined days is therefore needed to evaluate if the UFP observed during those days are coming from failed events or from pollution-related peaks (Buenrostro Mazon et al., 2016). A first analysis on undefined days reveals that on these days, particle growth stopped suddenly due to (i) a decrease of the total irradiance due to a cloud passing over the site (20 % of cases), (ii) a shift of the wind direction (17% of cases), or (iii) both parameters changing simultaneously (35 % of cases).

The shift of the wind orientation leading to a stop of the particle growth indicates that NPF events are associated with certain wind directions or air mass origins. To investigate this, HYSPLIT back trajectories were first sorted as a function of NPF event, non-event, and undefined days. Only back trajectories arriving between 09:00 and 14:00 UTC (period of NPF high occurrences) were selected for further analysis. During the NPF events, the predominant air masses were tracked back along the eastern North Sea region (Fig. 10a). Comparing these results to back trajectories for non-event days highlights a more continental influence. Indeed, most of the back trajectories during non-event days pass over large cities (Dunkirk, Paris, London, Rotterdam) before reaching Lille metropolis (Fig. 10b). Those air masses might then have been slightly enriched in primary precursor vapors. This result is consistent with previous results showing that "cleaner" air masses are associated with higher probability of NPF events (Bousiotis et al., 2019).

3.7 Nucleation strength factor

The nucleation strength factor ($NSF_{15.7–100}$) is calculated as the ratio of fine ($15.7 < D_p < 100$ nm) to accumulation ($100 < D_p < 800$ nm) particle concentrations observed during NPF event days over the same ratio observed during non-event days (Salma et al., 2017). Fine and accumulation mode particle number concentrations ($N_{15.7–100}$ and $N_{100–800}$) were retrieved from the SMPS data (Fig. 11a). The limited atmospheric residence time of fine particles (typically lower than 10 h, Seinfeld and Pandis, 2016) means that a large portion of the $N_{15.7–100}$ concentrations can be related to local emissions and/or formation processes, including NPF events. On the contrary, due to a longer residence time within the atmosphere (up to 10 d, Seinfeld and Pandis, 2016), $N_{100–800}$ is more related to large spatial and temporal scales. Therefore, the numerator represents the increase of $N_{15.7–100}$ relative to $N_{100–800}$ caused by all sources, while the denominator represents the same property due to all sources except NPF. The NSF method is based on the hypothesis that aerosol sources are similar from day to day and from season to season, excepting the sporadic occurrence of NPF. Considering the large number of NPF event (96) and non-event (432) days used to calculate $NSF_{15.7–100}$, one can assume that the sporadic/occasional (i.e., not observed on daily basis) sources of UFP other than NPF events (e.g., volcanic plumes) have little impact on the $NSF_{15.7–100}$ in comparison to the sources that are always active (such as traffic, industries, etc).

NSF is generally used to better assess the contribution of NPF to fine particle number concentrations relative to the regional background particle number concentrations. If the NSF ≈ 1, then the relative contribution of NPF to par-

Table 1. Correlation coefficients between different meteorological parameters (T, RH), nitrogen oxides (NO_x), black carbon concentrations from wood burning (BC_{wb}), and the total condensation sink (CS) during NPF event and non-event days for the 4-year period (2017–2020) and over the 09:00–14:00 UTC time window. High positive or negative correlations are marked in bold.

		CS	T	RH	NO_x	BC_{wb}
Event days	CS	1				
	T	**0.55**	1			
	RH	−0.39	−0.40	1		
	NO_x	−0.17	−0.24	0.48	1	
	BC_{wb}	0.19	−0.04	0.11	0.47	1
Non-event days	CS	1				
	T	0.06	1			
	RH	−0.03	−0.50	1		
	NO_x	0.30	−0.44	0.44	1	
	BC_{wb}	**0.67**	−0.37	0.28	**0.65**	1

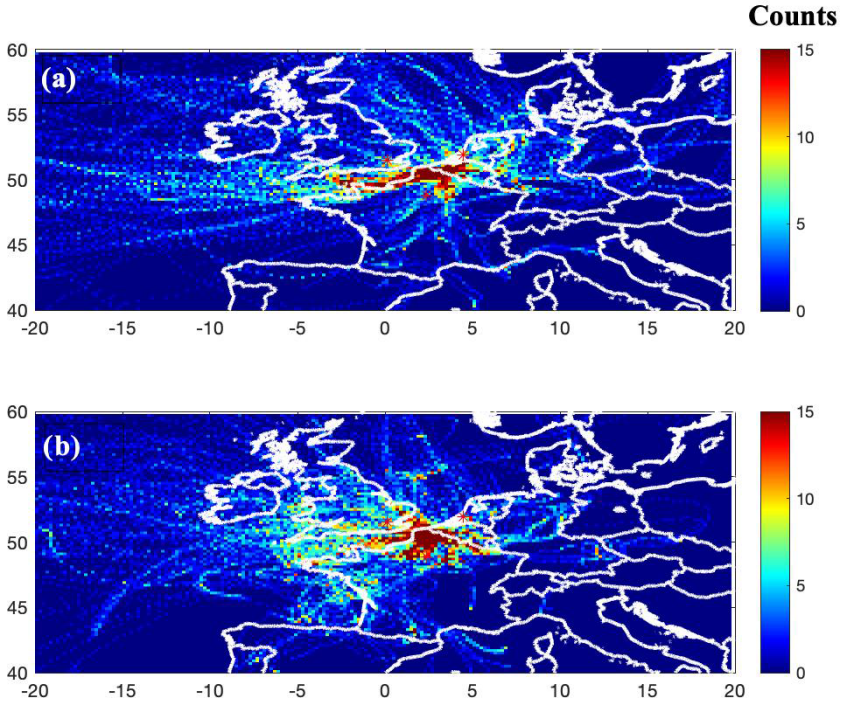

Figure 10. Three-day hourly back trajectories arriving at ATOLL between 09:00 and 14:00 UTC during **(a)** NPF event and **(b)** non-event days. Back-trajectories were calculated for each hour at ATOLL arriving at half the boundary layer height using GDAS 1° × 1° meteorological data. The color contour represents the back trajectory crossing counts in each grid cell (resolution 0.2° × 0.2°).

ticle number concentration with respect to other sources is negligible, as observed at the Granada (Spain) urban site (Casquero-Vera et al., 2021). Moreover, Salma et al. (2017) also defined two thresholds for $NSF_{6–100}$ to describe NPF contribution as a single source: a considerable contribution ($1 < NSF_{6–100} < 2$) or larger than all other sources together ($NSF_{6–100} > 2$). One should keep in mind that these thresholds were defined accordingly to the lower cut-off diameter originally set at 6 nm. As the lower cut-off diameter used in this study is a bit larger (15.7 instead of 6 nm) than the one used by Salma et al. (2017), the calculated $NSF_{15.7–100}$ would necessarily be underestimated in comparison to $NSF_{6–100}$ from Salma et al. (2017). The hourly median value of fine-to-accumulation particle concentration ratio was computed for NPF event and non-event days. Figure 10 shows the $NSF_{15.7–100}$ diel variation observed at ATOLL over 4 years of measurements.

During spring, the $NSF_{15.7–100}$ factor remains quite constant (about 1.5) during night and morning and peaks at 16:00 UTC to reach a maximum of 2.5 (Fig. 11b). This in-

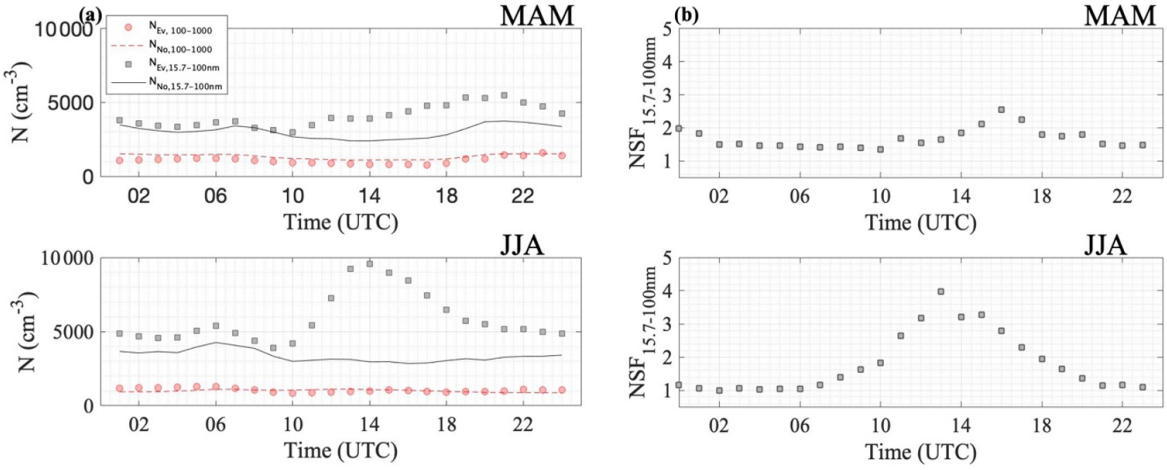

Figure 11. **(a)** Diel variations of fine ($15.7 < D_p < 100$ nm) and accumulation ($100 < D_p < 1000$ nm) mode particle number concentrations ($N_{15.7–100}$ in black and $N_{100–1000}$ in red) during MAM and JJA at the ATOLL site during the 2017–2020 period. The dots correspond to NPF event days, while the line correspond to non-event days. **(b)** Diel variations of the nucleation strength factor ($NSF_{15.7–100}$) for each season calculated from $N_{15.7–100}$ and $N_{100–800}$ observed during the 2017–2020 period.

dicates that NPF has a significant effect on particle number concentration only a few (2–3) hours after the averaged NPF starting time. During summer, the tendency of the $NSF_{15.7–100}$ is quite similar with a unique peak at 13:00 UTC (again 2–3 h after the averaged NPF starting time). At that time the median $NSF_{15.7–100}$ values reach 4, while from 21:00 to 06:00 UTC the $NSF_{15.7–100}$ remains low (averaged at 1.08). Therefore, during summer, the NPF contribution to particle number concentration is extremely high from 10:00 to 18:00 UTC and then negligible for the rest of the day in comparison to other sources.

Such $NSF_{10–100}$ diel variations were observed in other European cities (Budapest, Vienna, and Prague) with maximum values reaching 2.7, 2.3, and 3.4, respectively, for a lower cut-off diameter set at 10 nm (Németh et al., 2018). Moreover, Salma et al. (2017) reported $NSF_{6–100}$ peaks at midday varying from 2.2 and 2.7 for Budapest city center and from 2 to 7.2 for near city background for each season with $NSF_{6–100}$ maximum reached during winter. The nucleation frequency during winter in Budapest is low (< 10 %), similarly to our observations; however, the impact of these limited number of NPF events on particle number concentrations is high. It may be mentioned that the $NSF_{15.7–100}$ factor over ATOLL peaked at 3.5 and 2.3 during winter and fall, respectively.

As previously shown by Sebastian et al. (2021), NPF events can also play a major role on the Earth's radiative budget when the newly formed particles grow to climate-relevant sizes (50–100 nm). In order to understand the NPF influence on these particles, the $NSF_{50–100}$ was also calculated (see Fig. S3). The results show a large increase of up to 1.6 of the $NSF_{50–100}$ in the early afternoon for both seasons. This suggests a potential impact on CCN concentrations that needs to be further studied with proper instrumentation.

4 Conclusions

This study was based on a 4-year (2017–2020) dataset collected at the ATOLL site, in close vicinity of the city of Lille, northern France, to study NPF occurrence over a peri-urban site. The results highlight a strong seasonal variation of the NPF event frequency, with a maximum occurrence observed during spring (15 %) and summer (19 %). The undefined cases, which correspond to bursts of UFP that do not grow, are much more frequent (40 % on average) than NPF events all year long. The highest frequency (68 %) is observed in August and the lowest one (17 %) in February. The interruption of particle growth during undefined events can be mostly attributed to changes in environmental conditions (irradiance and wind direction).

The seasonal variation of NPF parameters was also clearly observed and associated with environmental parameters. High temperature ($T > 295$ K), low RH (RH < 45 %), and high solar radiation favor the occurrence of NPF events at ATOLL. The presence of clouds, linked to a decrease of solar radiation, also limits the NPF event occurrences. Moreover, NPF events start earlier in the morning from May to September, most probably related to variations in sunrise time. The GR calculated between 15.7 and 30 nm ($GR_{15.7–30\,nm}$) ranges from 1.8 nm h^{-1} in March up to 10.9 nm h^{-1} in July. The $GR_{15.7–30\,nm}$ was also found to be positively correlated with temperature. This correlation might be related to larger emissions of biogenic precursors at higher temperatures, including monoterpenes known to favor the occurrence of NPF events (Kulmala et al., 2004).

Relatively high values of CS ($> 2 \times 10^{-2}\,s^{-1}$) are reported during NPF events as well as during non-event days. These results suggest that high CS values are not limiting the NPF event occurrence, consistent with recent studies focusing on NPF events over urban sites (Deng et al., 2020; Hussein et al., 2020; Pushpawela et al., 2018). Looking more closely before the NPF onset (from 07:00 to 09:00 UTC), $CS_{07:00–09:00}$ values are larger by 16 % during non-event days. Interestingly, CS tends to increase during NPF event days (especially in summer) and size-resolved CS clearly shows a peak shift from 150 nm during non-event days to 50 nm during NPF event days, thus highlighting the strong contribution of newly formed particles on CS.

Air mass back trajectories (HYSPLIT) arriving over ATOLL during NPF event days revealed a specific path along the eastern North Sea region with only a small fraction passing over any continental area and therefore not crossing many anthropogenic sources, while most of the back trajectories during non-event days pass over large cities (Dunkirk, Paris, London, Rotterdam) before reaching Lille. The precursor vapor concentrations and probably their nature might differ from both "clean" and "polluted" air masses and therefore promote or inhibit NPF event occurrences, a point which requires further investigation.

The impact of NPF events on particle number concentrations has been estimated through the nucleation strength factor (NSF; Salma et al., 2017). The $NSF_{15.7–100\,nm}$ diel variation was calculated for spring and summer occurring 2 to 3 h after the average NPF starting time and reaching 1.5 and 4 during spring and summer, respectively. The extremely large $NSF_{15.7–100\,nm}$ values observed during summer evidence the very high NPF contribution to the fine particle ($D_p < 100$ nm) number concentrations in comparison to other regional sources. Recently, Ren et al. (2021) highlighted the strong impact of newly formed particles from NPF on CCN especially at sites close to anthropogenic sources, such as ATOLL. In future studies, the impact of local vertical dynamics such as the effect of the boundary layer dynamics as in Lampilahti et al. (2021, 2020) as well as the CCN enhancement factor will be analyzed.

Data availability. ATOLL measurements are available through the EBAS database (https://ebas-data.nilu.no/Pages/DataSetList.aspx?key=F9603747DC7D43F092A6CA18C91BDF09, last access: 2 January 2023; Crumeyrolle, 2022a) and SMPS data before 2020 through https://doi.org/10.5281/zenodo.6794562 (Crumeyrolle, 2022b). GDAS files for back trajectory calculations are available on demand at https://www.arl.noaa.gov/hysplit/ (last access: 22 September 2022; NOAA, 2022). NO_x data can be requested through the ATMO website: https://data-atmo-hdf.opendata.arcgis.com (last access: 3 March 2022; Atmo Hauts-de-France, 2022).

Supplement. The supplement related to this article is available online at: https://doi.org/10.5194/acp-23-183-2023-supplement.

Author contributions. SC performed the data analysis and wrote the paper. AVG and SC analyzed the data. ET and MC maintain the measurement platform. VR and ET are responsible for the ACSM measurements. JFdB and ET are responsible for the Aethalometer measurements. NF and FA are responsible for radiation measurements. JSSK, CR, NV, and IC provided supervision. All authors contributed to the discussion of the results and provided comments on the paper.

Competing interests. The contact author has declared that none of the authors has any competing interests.

Disclaimer. Publisher's note: Copernicus Publications remains neutral with regard to jurisdictional claims in published maps and institutional affiliations.

Acknowledgements. This research was supported by the French National Research Agency (ANR) under the MABCaM (ANR-16-CE04-0009) contract. Part of the instrumental system has been financially supported by the CaPPA project (Chemical and Physical Properties of the Atmosphere), which is funded by the French National Research Agency (ANR) through the PIA (Programme d'Investissement d'Avenir) under contract "ANR-11-LABX-0005-01" and by the Regional Council "Hauts-de-France". ATOLL is a French component of the Aerosol, Clouds and Trace Gases Research Infrastructure (ACTRIS, https://www.actris.eu/, last access: 1 October 2022), and the particle chemical composition measurements are also supported by the CARA program of the LCSQA funded by the French Ministry of Environment. The authors also thank the Région Hauts-de-France, the Ministère de l'Enseignement Supérieur et de la Recherche (CPER Climibio), and the European Fund for Regional Economic Development for their financial support. The authors gratefully acknowledge the NOAA Air Resources Laboratory (ARL) for the provision of the HYSPLIT transport and dispersion model and/or READY website (https://www.ready.noaa.gov, last access: 29 June 2021) used in this publication. We thank François Thieuleux for ECMWF data sharing during this work.

Financial support. This research has been supported by the Agence Nationale de la Recherche (grant nos. ANR-16-CE04-0009 and ANR-11-LABX-0005-01), the Regional Council "Hauts-de-France", the CARA program of the LCSQA funded by the French Ministry of Environment, the Ministère de l'Enseignement Supérieur et de la Recherche (CPER Climibio), and the European Fund for Regional Economic Development.

Review statement. This paper was edited by Luis A. Ladino and reviewed by two anonymous referees.

References

Atmo Hauts-de-France: NO_x data, https://data-atmo-hdf.opendata.arcgis.com, last access: 3 March 2022.

Barreira, L. M. F., Helin, A., Aurela, M., Teinilä, K., Friman, M., Kangas, L., Niemi, J. V., Portin, H., Kousa, A., Pirjola, L., Rönkkö, T., Saarikoski, S., and Timonen, H.: In-depth characterization of submicron particulate matter inter-annual variations at a street canyon site in northern Europe, Atmos. Chem. Phys., 21, 6297–6314, https://doi.org/10.5194/acp-21-6297-2021, 2021.

Berland, K., Rose, C., Pey, J., Culot, A., Freney, E., Kalivitis, N., Kouvarakis, G., Cerro, J. C., Mallet, M., Sartelet, K., Beckmann, M., Bourriane, T., Roberts, G., Marchand, N., Mihalopoulos, N., and Sellegri, K.: Spatial extent of new particle formation events over the Mediterranean Basin from multiple ground-based and airborne measurements, Atmos. Chem. Phys., 17, 9567–9583, https://doi.org/10.5194/acp-17-9567-2017, 2017.

Boichu, M., Favez, O., Riffault, V., Petit, J.-E., Zhang, Y., Brogniez, C., Sciare, J., Chiapello, I., Clarisse, L., Zhang, S., Pujol-Söhne, N., Tison, E., Delbarre, H., and Goloub, P.: Large-scale particulate air pollution and chemical fingerprint of volcanic sulfate aerosols from the 2014–2015 Holuhraun flood lava eruption of Bárðarbunga volcano (Iceland), Atmos. Chem. Phys., 19, 14253–14287, https://doi.org/10.5194/acp-19-14253-2019, 2019.

Bousiotis, D., Dall'Osto, M., Beddows, D. C. S., Pope, F. D., and Harrison, R. M.: Analysis of new particle formation (NPF) events at nearby rural, urban background and urban roadside sites, Atmos. Chem. Phys., 19, 5679–5694, https://doi.org/10.5194/acp-19-5679-2019, 2019.

Bousiotis, D., Brean, J., Pope, F. D., Dall'Osto, M., Querol, X., Alastuey, A., Perez, N., Petäjä, T., Massling, A., Nøjgaard, J. K., Nordstrøm, C., Kouvarakis, G., Vratolis, S., Eleftheriadis, K., Niemi, J. V., Portin, H., Wiedensohler, A., Weinhold, K., Merkel, M., Tuch, T., and Harrison, R. M.: The effect of meteorological conditions and atmospheric composition in the occurrence and development of new particle formation (NPF) events in Europe, Atmos. Chem. Phys., 21, 3345–3370, https://doi.org/10.5194/acp-21-3345-2021, 2021.

Bovchaliuk, V., Goloub, P., Podvin, T., Veselovskii, I., Tanre, D., Chaikovsky, A., Dubovik, O., Mortier, A., Lopatin, A., Korenskiy, M., and Victori, S.: Comparison of aerosol properties retrieved using GARRLiC, LIRIC, and Raman algorithms applied to multi-wavelength lidar and sun/sky-photometer data, Atmos. Meas. Tech., 9, 3391–3405, https://doi.org/10.5194/amt-9-3391-2016, 2016.

Buenrostro Mazon, S., Riipinen, I., Schultz, D. M., Valtanen, M., Dal Maso, M., Sogacheva, L., Junninen, H., Nieminen, T., Kerminen, V.-M., and Kulmala, M.: Classifying previously undefined days from eleven years of aerosol-particle-size distribution data from the SMEAR II station, Hyytiälä, Finland, Atmos. Chem. Phys., 9, 667–676, https://doi.org/10.5194/acp-9-667-2009, 2009.

Buenrostro Mazon, S., Kontkanen, J., Manninen, H. E., Nieminen, T., Kerminen, V.-M., and Kulmala, M.: A long-term comparison of nighttime cluster events and daytime ion formation in a boreal forest, Boreal Environ. Res., 21, 242–261, 2016.

Casquero-Vera, J. A., Lyamani, H., Titos, G., Minguillón, M. C., Dada, L., Alastuey, A., Querol, X., Petäjä, T., Olmo, F. J., and Alados-Arboledas, L.: Quantifying traffic, biomass burning and secondary source contributions to atmospheric particle number concentrations at urban and suburban sites, Sci. Total Environ., 768, 145282, https://doi.org/10.1016/j.scitotenv.2021.145282, 2021.

Chen, G., Canonaco, F., Tobler, A., Aas, W., Alastuey, A., Allan, J., Atabakhsh, S., Aurela, M., Baltensperger, U., Bougiatioti, A., De Brito, J. F., Ceburnis, D., Chazeau, B., Chebaicheb, H., Daellenbach, K. R., Ehn, M., El Haddad, I., Eleftheriadis, K., Favez, O., Flentje, H., Font, A., Fossum, K., Freney, E., Gini, M., Green, D. C., Heikkinen, L., Herrmann, H., Kalogridis, A.-C., Keernik, H., Lhotka, R., Lin, C., Lunder, C., Maasikmets, M., Manousakas, M. I., Marchand, N., Marin, C., Marmureanu, L., Mihalopoulos, N., Močnik, G., Nęcki, J., O'Dowd, C., Ovadnevaite, J., Peter, T., Petit, J.-E., Pikridas, M., Matthew Platt, S., Pokorná, P., Poulain, L., Priestman, M., Riffault, V., Rinaldi, M., Różański, K., Schwarz, J., Sciare, J., Simon, L., Skiba, A., Slowik, J. G., Sosedova, Y., Stavroulas, I., Styszko, K., Teinemaa, E., Timonen, H., Tremper, A., Vasilescu, J., Via, M., Vodička, P., Wiedensohler, A., Zografou, O., Cruz Minguillón, M., and Prévôt, A. S. H.: European Aerosol Phenomenology – 8: Harmonised Source Apportionment of Organic Aerosol using 22 Year-long ACSM/AMS Datasets, Environ. Int., 166, 107325, https://doi.org/10.1016/j.envint.2022.107325, 2022.

Clifford, S., Mazaheri, M., Salimi, F., Ezz, W. N., Yeganeh, B., Low-Choy, S., Walker, K., Mengersen, K., Marks, G. B., and Morawska, L.: Effects of exposure to ambient ultrafine particles on respiratory health and systemic inflammation in children, Environ. Int., 114, 167–180, https://doi.org/10.1016/j.envint.2018.02.019, 2018.

Crumeyrolle, S.: Data for acp-2022-436, Version 1, EBAS [data set], https://ebas-data.nilu.no/Pages/DataSetList.aspx?key=F9603747DC7D43F092A6CA18C91BDF09 (last access: 2 January 2023), 2022a.

Crumeyrolle, S.: Data for acp-2022-436, Version 1, Zenodo [data set], https://doi.org/10.5281/zenodo.6794562, 2022b.

Cuesta-Mosquera, A., Močnik, G., Drinovec, L., Müller, T., Pfeifer, S., Minguillón, M. C., Briel, B., Buckley, P., Dudoitis, V., Fernández-García, J., Fernández-Amado, M., Ferreira De Brito, J., Riffault, V., Flentje, H., Heffernan, E., Kalivitis, N., Kalogridis, A.-C., Keernik, H., Marmureanu, L., Luoma, K., Marinoni, A., Pikridas, M., Schauer, G., Serfozo, N., Servomaa, H., Titos, G., Yus-Díez, J., Zioła, N., and Wiedensohler, A.: Intercomparison and characterization of 23 Aethalometers under laboratory and ambient air conditions: procedures and unit-to-unit variabilities, Atmos. Meas. Tech., 14, 3195–3216, https://doi.org/10.5194/amt-14-3195-2021, 2021.

Dada, L., Paasonen, P., Nieminen, T., Buenrostro Mazon, S., Kontkanen, J., Peräkylä, O., Lehtipalo, K., Hussein, T., Petäjä, T., Kerminen, V.-M., Bäck, J., and Kulmala, M.: Long-term analysis of clear-sky new particle formation events and nonevents in Hyytiälä, Atmos. Chem. Phys., 17, 6227–6241, https://doi.org/10.5194/acp-17-6227-2017, 2017.

Dal Maso, M., Kulmala, M., Riipinen, I., Wagner, R., Hussein, T., Aalto, P. P., and Lehtinen, K. E. J.: Formation and growth of fresh atmospheric aerosols: Eight years of aerosol size distribution data from SMEAR II, Hyytiälä, Finland, Boreal Environ. Res., 10, 323–336, 2005.

Dall'Osto, M., Beddows, D. C. S., Asmi, A., Poulain, L., Hao, L., Freney, E., Allan, J. D., Canagaratna, M., Crippa, M., Bianchi,

F., de Leeuw, G., Eriksson, A., Swietlicki, E., Hansson, H. C., Henzing, J. S., Granier, C., Zemankova, K., Laj, P., Onasch, T., Prevot, A., Putaud, J. P., Sellegri, K., Vidal, M., Virtanen, A., Simo, R., Worsnop, D., O'Dowd, C., Kulmala, M., and Harrison, R. M.: Novel insights on new particle formation derived from a pan-european observing system, Sci. Rep., 8, 1482, https://doi.org/10.1038/s41598-017-17343-9, 2018.

Deng, C., Fu, Y., Dada, L., Yan, C., Cai, R., Yang, D., Zhou, Y., Yin, R., Lu, Y., Li, X., Qiao, X., Fan, X., Nie, W., Kontkanen, J., Kangasluoma, J., Chu, B., Ding, A., Kerminen, V.-M., Paasonen, P., Worsnop, D. R., Bianchi, F., Liu, Y., Zheng, J., Wang, L., Kulmala, M., and Jiang, J.: Seasonal Characteristics of New Particle Formation and Growth in Urban Beijing, Environ. Sci. Technol., 54, 8547–8557, https://doi.org/10.1021/acs.est.0c00808, 2020.

Dos Santos, V. N., Herrmann, E., Manninen, H. E., Hussein, T., Hakala, J., Nieminen, T., Aalto, P. P., Merkel, M., Wiedensohler, A., Kulmala, M., Petäjä, T., and Hämeri, K.: Variability of air ion concentrations in urban Paris, Atmos. Chem. Phys., 15, 13717–13737, https://doi.org/10.5194/acp-15-13717-2015, 2015.

Duplissy, J., Merikanto, J., Franchin, A., Tsagkogeorgas, G., Kangasluoma, J., Wimmer, D., Vuollekoski, H., Schobesberger, S., Lehtipalo, K., Flagan, R. C., Brus, D., Donahue, N. M., Vehkamäki, H., Almeida, J., Amorim, A., Barmet, P., Bianchi, F., Breitenlechner, M., Dunne, E. M., Guida, R., Henschel, H., Junninen, H., Kirkby, J., Kürten, A., Kupc, A., Määttänen, A., Makhmutov, V., Mathot, S., Nieminen, T., Onnela, A., Praplan, A. P., Riccobono, F., Rondo, L., Steiner, G., Tome, A., Walther, H., Baltensperger, U., Carslaw, K. S., Dommen, J., Hansel, A., Petäjä, T., Sipilä, M., Stratmann, F., Vrtala, A., Wagner, P. E., Worsnop, D. R., Curtius, J., and Kulmala, M.: Effect of ions on sulfuric acid-water binary particle formation: 2. Experimental data and comparison with QC-normalized classical nucleation theory: BINARY PARTICLE FORMATION EXPERIMENTS, J. Geophys. Res.-Atmos., 121, 1752–1775, https://doi.org/10.1002/2015JD023539, 2016.

Fick, J., Pommer, L., Nilsson, C., and Andersson, B.: Effect of OH radicals, relative humidity, and time on the composition of the products formed in the ozonolysis of α-pinene, Atmos. Environ., 37, 4087–4096, https://doi.org/10.1016/S1352-2310(03)00522-3, 2003.

Fuks, N. A. and Sutugin, A. G.: Highly Dispersed Aerosols, Ann Arbor Science Publishers, 116 pp., ISBN 9780706507607, 1970.

Größ, J., Hamed, A., Sonntag, A., Spindler, G., Manninen, H. E., Nieminen, T., Kulmala, M., Hõrrak, U., Plass-Dülmer, C., Wiedensohler, A., and Birmili, W.: Atmospheric new particle formation at the research station Melpitz, Germany: connection with gaseous precursors and meteorological parameters, Atmos. Chem. Phys., 18, 1835–1861, https://doi.org/10.5194/acp-18-1835-2018, 2018.

Hamed, A., Korhonen, H., Sihto, S.-L., Joutsensaari, J., Järvinen, H., Petäjä, T., Arnold, F., Nieminen, T., Kulmala, M., Smith, J. N., Lehtinen, K. E. J., and Laaksonen, A.: The role of relative humidity in continental new particle formation, J. Geophys. Res., 116, D03202, https://doi.org/10.1029/2010JD014186, 2011.

Heinritzi, M., Dada, L., Simon, M., Stolzenburg, D., Wagner, A. C., Fischer, L., Ahonen, L. R., Amanatidis, S., Baalbaki, R., Baccarini, A., Bauer, P. S., Baumgartner, B., Bianchi, F., Brilke, S., Chen, D., Chiu, R., Dias, A., Dommen, J., Duplissy, J., Finkenzeller, H., Frege, C., Fuchs, C., Garmash, O., Gordon, H., Granzin, M., El Haddad, I., He, X., Helm, J., Hofbauer, V., Hoyle, C. R., Kangasluoma, J., Keber, T., Kim, C., Kürten, A., Lamkaddam, H., Laurila, T. M., Lampilahti, J., Lee, C. P., Lehtipalo, K., Leiminger, M., Mai, H., Makhmutov, V., Manninen, H. E., Marten, R., Mathot, S., Mauldin, R. L., Mentler, B., Molteni, U., Müller, T., Nie, W., Nieminen, T., Onnela, A., Partoll, E., Passananti, M., Petäjä, T., Pfeifer, J., Pospisilova, V., Quéléver, L. L. J., Rissanen, M. P., Rose, C., Schobesberger, S., Scholz, W., Scholze, K., Sipilä, M., Steiner, G., Stozhkov, Y., Tauber, C., Tham, Y. J., Vazquez-Pufleau, M., Virtanen, A., Vogel, A. L., Volkamer, R., Wagner, R., Wang, M., Weitz, L., Wimmer, D., Xiao, M., Yan, C., Ye, P., Zha, Q., Zhou, X., Amorim, A., Baltensperger, U., Hansel, A., Kulmala, M., Tomé, A., Winkler, P. M., Worsnop, D. R., Donahue, N. M., Kirkby, J., and Curtius, J.: Molecular understanding of the suppression of new-particle formation by isoprene, Atmos. Chem. Phys., 20, 11809–11821, https://doi.org/10.5194/acp-20-11809-2020, 2020.

Hussein, T., Atashi, N., Sogacheva, L., Hakala, S., Dada, L., Petäjä, T., and Kulmala, M.: Characterization of Urban New Particle Formation in Amman – Jordan, Atmosphere, 11, 79, https://doi.org/10.3390/atmos11010079, 2020.

Jokinen, V. and Mäkelä, J. M.: Closed-loop arrangement with critical orifice for DMA sheath/excess flow system, J. Aerosol Sci., 28, 643–648,https://doi.org/10.1016/S0021-8502(96)00457-0, 1997.

Kalkavouras, P., Bossioli, E., Bezantakos, S., Bougiatioti, A., Kalivitis, N., Stavroulas, I., Kouvarakis, G., Protonotariou, A. P., Dandou, A., Biskos, G., Mihalopoulos, N., Nenes, A., and Tombrou, M.: New particle formation in the southern Aegean Sea during the Etesians: importance for CCN production and cloud droplet number, Atmos. Chem. Phys., 17, 175–192, https://doi.org/10.5194/acp-17-175-2017, 2017.

Kanawade, V. P., Sebastian, M., Hooda, R. K., and Hyvärinen, A.-P.: Atmospheric new particle formation in India: Current understanding and knowledge gaps, Atmos. Environ., 270, 118894, https://doi.org/10.1016/j.atmosenv.2021.118894, 2022.

Kerminen, V.-M., Pirjola, L., and Kulmala, M.: How significantly does coagulational scavenging limit atmospheric particle production?, J. Geophys. Res., 106, 24119–24125, https://doi.org/10.1029/2001JD000322, 2001.

Kerminen, V.-M., Chen, X., Vakkari, V., Petäjä, T., Kulmala, M., and Bianchi, F.: Atmospheric new particle formation and growth: review of field observations, Environ. Res. Lett., 13, 103003, https://doi.org/10.1088/1748-9326/aadf3c, 2018.

Kontkanen, J., Järvinen, E., Manninen, H. E., Lehtipalo, K., Kangasluoma, J., Decesari, S., Gobbi, G. P., Laaksonen, A., Petäjä, T., and Kulmala, M.: High concentrations of sub-3 nm clusters and frequent new particle formation observed in the Po Valley, Italy, during the PEGASOS 2012 campaign, Atmos. Chem. Phys., 16, 1919–1935, https://doi.org/10.5194/acp-16-1919-2016, 2016.

Kontkanen, J., Lehtipalo, K., Ahonen, L., Kangasluoma, J., Manninen, H. E., Hakala, J., Rose, C., Sellegri, K., Xiao, S., Wang, L., Qi, X., Nie, W., Ding, A., Yu, H., Lee, S., Kerminen, V.-M., Petäjä, T., and Kulmala, M.: Measurements of sub-3 nm particles using a particle size magnifier in different environments: from clean mountain top to polluted megacities, Atmos. Chem. Phys., 17, 2163–2187, https://doi.org/10.5194/acp-17-2163-2017, 2017.

Kulmala, M.: Atmospheric science. How particles nucleate and grow, Science, 302, 1000–1001, https://doi.org/10.1126/science.1090848, 2003.

Kulmala, M., Dal Maso, M., Mäkelä, J. M., Pirjola, L., Väkevä, M., Aalto, P., Miikkulainen, P., Hämeri, K., and O'Dowd, C. D.: On the formation, growth and composition of nucleation mode particles, Tellus B, 53, 479–490, https://doi.org/10.1034/j.1600-0889.2001.530411.x, 2001.

Kulmala, M., Vehkamäki, H., Petäjä, T., Dal Maso, M., Lauri, A., Kerminen, V.-M., Birmili, W., and McMurry, P. H.: Formation and growth rates of ultrafine atmospheric particles: a review of observations, J. Aerosol Sci., 35, 143–176, https://doi.org/10.1016/j.jaerosci.2003.10.003, 2004.

Kulmala, M., Petäjä, T., Nieminen, T., Sipilä, M., Manninen, H. E., Lehtipalo, K., Maso, M. D., Aalto, P. P., Junninen, H., Paasonen, P., Riipinen, I., Lehtinen, K. E. J., Laaksonen, A., and Kerminen, V. M.: Measurement of the nucleation of atmospheric aerosol particles, Nat. Protoc., 7, 1651–1667, https://doi.org/10.1038/nprot.2012.091, 2012.

Kulmala, M., Petäjä, T., Ehn, M., Thornton, J., Sipilä, M., Worsnop, D. R., and Kerminen, V.-M.: Chemistry of Atmospheric Nucleation: On the Recent Advances on Precursor Characterization and Atmospheric Cluster Composition in Connection with Atmospheric New Particle Formation, Annu. Rev. Phys. Chem., 65, 21–37, https://doi.org/10.1146/annurev-physchem-040412-110014, 2014.

Kulmala, M., Kerminen, V.-M., Petäjä, T., Ding, A. J., and Wang, L.: Atmospheric gas-to-particle conversion: why NPF events are observed in megacities?, Faraday Discuss., 200, 271–288, https://doi.org/10.1039/C6FD00257A, 2017.

Kulmala, M., Junninen, H., Dada, L., Salma, I., Weidinger, T., Thén, W., Vörösmarty, M., Komsaare, K., Stolzenburg, D., Cai, R., Yan, C., Li, X., Deng, C., Jiang, J., Petäjä, T., Nieminen, T., and Kerminen, V.-M.: Quiet New Particle Formation in the Atmosphere, Front. Environ. Sci., 10, 912385, https://doi.org/10.3389/fenvs.2022.912385, 2022.

Kurtén, T., Torpo, L., Ding, C.-G., Vehkamäki, H., Sundberg, M. R., Laasonen, K., and Kulmala, M.: A density functional study on water-sulfuric acid-ammonia clusters and implications for atmospheric cluster formation, J. Geophys. Res., 112, D04210, https://doi.org/10.1029/2006JD007391, 2007.

Laj, P., Bigi, A., Rose, C., Andrews, E., Lund Myhre, C., Collaud Coen, M., Lin, Y., Wiedensohler, A., Schulz, M., Ogren, J. A., Fiebig, M., Gliß, J., Mortier, A., Pandolfi, M., Petäja, T., Kim, S.-W., Aas, W., Putaud, J.-P., Mayol-Bracero, O., Keywood, M., Labrador, L., Aalto, P., Ahlberg, E., Alados Arboledas, L., Alastuey, A., Andrade, M., Artíñano, B., Ausmeel, S., Arsov, T., Asmi, E., Backman, J., Baltensperger, U., Bastian, S., Bath, O., Beukes, J. P., Brem, B. T., Bukowiecki, N., Conil, S., Couret, C., Day, D., Dayantolis, W., Degorska, A., Eleftheriadis, K., Fetfatzis, P., Favez, O., Flentje, H., Gini, M. I., Gregorič, A., Gysel-Beer, M., Hallar, A. G., Hand, J., Hoffer, A., Hueglin, C., Hooda, R. K., Hyvärinen, A., Kalapov, I., Kalivitis, N., Kasper-Giebl, A., Kim, J. E., Kouvarakis, G., Kranjc, I., Krejci, R., Kulmala, M., Labuschagne, C., Lee, H.-J., Lihavainen, H., Lin, N.-H., Löschau, G., Luoma, K., Marinoni, A., Martins Dos Santos, S., Meinhardt, F., Merkel, M., Metzger, J.-M., Mihalopoulos, N., Nguyen, N. A., Ondracek, J., Pérez, N., Perrone, M. R., Petit, J.-E., Picard, D., Pichon, J.-M., Pont, V., Prats, N., Prenni, A., Reisen, F., Romano, S., Sellegri, K., Sharma, S., Schauer, G., Sheridan, P., Sherman, J. P., Schütze, M., Schwerin, A., Sohmer, R., Sorribas, M., Steinbacher, M., Sun, J., Titos, G., Toczko, B., Tuch, T., Tulet, P., Tunved, P., Vakkari, V., Velarde, F., Velasquez, P., Villani, P., Vratolis, S., Wang, S.-H., Weinhold, K., Weller, R., Yela, M., Yus-Diez, J., Zdimal, V., Zieger, P., and Zikova, N.: A global analysis of climate-relevant aerosol properties retrieved from the network of Global Atmosphere Watch (GAW) near-surface observatories, Atmos. Meas. Tech., 13, 4353–4392, https://doi.org/10.5194/amt-13-4353-2020, 2020.

Lampilahti, J., Manninen, H. E., Leino, K., Väänänen, R., Manninen, A., Buenrostro Mazon, S., Nieminen, T., Leskinen, M., Enroth, J., Bister, M., Zilitinkevich, S., Kangasluoma, J., Järvinen, H., Kerminen, V.-M., Petäjä, T., and Kulmala, M.: Roll vortices induce new particle formation bursts in the planetary boundary layer, Atmos. Chem. Phys., 20, 11841–11854, https://doi.org/10.5194/acp-20-11841-2020, 2020.

Lampilahti, J., Leino, K., Manninen, A., Poutanen, P., Franck, A., Peltola, M., Hietala, P., Beck, L., Dada, L., Quéléver, L., Öhrnberg, R., Zhou, Y., Ekblom, M., Vakkari, V., Zilitinkevich, S., Kerminen, V.-M., Petäjä, T., and Kulmala, M.: Aerosol particle formation in the upper residual layer, Atmos. Chem. Phys., 21, 7901–7915, https://doi.org/10.5194/acp-21-7901-2021, 2021.

Liao, L., Kerminen, V.-M., Boy, M., Kulmala, M., and Dal Maso, M.: Temperature influence on the natural aerosol budget over boreal forests, Atmos. Chem. Phys., 14, 8295–8308, https://doi.org/10.5194/acp-14-8295-2014, 2014.

Lyubovtseva, Y. S., Sogacheva, L., Maso, M. D., Bonn, B., Keronen, P., and Kulmala, M.: Seasonal variations of trace gases, meteorological parameters, and formation of aerosols in boreal forests, Boreal Environ. Res., 10, 18 pp., 2005.

Marten, R., Xiao, M., Rörup, B., Wang, M., Kong, W., He, X.-C., Stolzenburg, D., Pfeifer, J., Marie, G., Wang, D. S., Scholz, W., Baccarini, A., Lee, C. P., Amorim, A., Baalbaki, R., Bell, D. M., Bertozzi, B., Caudillo, L., Chu, B., Dada, L., Duplissy, J., Finkenzeller, H., Carracedo, L. G., Granzin, M., Hansel, A., Heinritzi, M., Hofbauer, V., Kemppainen, D., Kürten, A., Lampimäki, M., Lehtipalo, K., Makhmutov, V., Manninen, H. E., Mentler, B., Petäjä, T., Philippov, M., Shen, J., Simon, M., Stozhkov, Y., Tomé, A., Wagner, A. C., Wang, Y., Weber, S. K., Wu, Y., Zauner-Wieczorek, M., Curtius, J., Kulmala, M., Möhler, O., Volkamer, R., Winkler, P. M., Worsnop, D. R., Dommen, J., Flagan, R. C., Kirkby, J., Donahue, N. M., Lamkaddam, H., Baltensperger, U., and Haddad, I. E.: Survival of newly formed particles in haze conditions, Environ. Sci.: Atmos., 2, 491–499, https://doi.org/10.1039/D2EA00007E, 2022.

Merikanto, J., Duplissy, J., Määttänen, A., Henschel, H., Donahue, N. M., Brus, D., Schobesberger, S., Kulmala, M., and Vehkamäki, H.: Effect of ions on sulfuric acid-water binary particle formation: 1. Theory for kinetic- and nucleation-type particle formation and atmospheric implications, J. Geophys. Res.-Atmos., 121, 1736–1751, https://doi.org/10.1002/2015JD023538, 2016.

Middlebrook, A. M., Bahreini, R., Jimenez, J. L., and Canagaratna, M. R.: Evaluation of Composition-Dependent Collection Efficiencies for the Aerodyne Aerosol Mass Spectrometer using Field Data, Aerosol Sci. Tech., 46, 258–271, https://doi.org/10.1080/02786826.2011.620041, 2012.

Mortier, A., Goloub, P., Podvin, T., Deroo, C., Chaikovsky, A., Ajtai, N., Blarel, L., Tanre, D., and Derimian, Y.: Detection and characterization of volcanic ash plumes over Lille during the Eyjafjallajökull eruption, Atmos. Chem. Phys., 13, 3705–3720, https://doi.org/10.5194/acp-13-3705-2013, 2013.

Németh, Z., Rosati, B., Zíková, N., Salma, I., Bozó, L., Dameto de España, C., Schwarz, J., Ždímal, V., and Wonaschütz, A.: Comparison of atmospheric new particle formation events in three Central European cities, Atmos. Environ., 178, 191–197, https://doi.org/10.1016/j.atmosenv.2018.01.035, 2018.

Nieminen, T., Kerminen, V.-M., Petäjä, T., Aalto, P. P., Arshinov, M., Asmi, E., Baltensperger, U., Beddows, D. C. S., Beukes, J. P., Collins, D., Ding, A., Harrison, R. M., Henzing, B., Hooda, R., Hu, M., Hõrrak, U., Kivekäs, N., Komsaare, K., Krejci, R., Kristensson, A., Laakso, L., Laaksonen, A., Leaitch, W. R., Lihavainen, H., Mihalopoulos, N., Németh, Z., Nie, W., O'Dowd, C., Salma, I., Sellegri, K., Svenningsson, B., Swietlicki, E., Tunved, P., Ulevicius, V., Vakkari, V., Vana, M., Wiedensohler, A., Wu, Z., Virtanen, A., and Kulmala, M.: Global analysis of continental boundary layer new particle formation based on long-term measurements, Atmos. Chem. Phys., 18, 14737–14756, https://doi.org/10.5194/acp-18-14737-2018, 2018.

NOAA: Hysplit, https://www.arl.noaa.gov/hysplit/, last access: 22 September 2022.

Ohlwein, S., Kappeler, R., Kutlar Joss, M., Künzli, N., and Hoffmann, B.: Health effects of ultrafine particles: a systematic literature review update of epidemiological evidence, Int. J. Public Health, 64, 547–559, https://doi.org/10.1007/s00038-019-01202-7, 2019.

Paasonen, P., Peltola, M., Kontkanen, J., Junninen, H., Kerminen, V.-M., and Kulmala, M.: Comprehensive analysis of particle growth rates from nucleation mode to cloud condensation nuclei in boreal forest, Atmos. Chem. Phys., 18, 12085–12103, https://doi.org/10.5194/acp-18-12085-2018, 2018.

Peng, Y., Dong, Y., Li, X., Liu, X., Dai, J., Chen, C., Dong, Z., Du, C., and Wang, Z.: Different Characteristics of New Particle Formation Events at Two Suburban Sites in Northern China, Atmosphere, 8, 258, https://doi.org/10.3390/atmos8120258, 2017.

Pierce, J. R. and Adams, P. J.: Uncertainty in global CCN concentrations from uncertain aerosol nucleation and primary emission rates, Atmos. Chem. Phys., 9, 1339–1356, https://doi.org/10.5194/acp-9-1339-2009, 2009.

Pushpawela, B., Jayaratne, R., and Morawska, L.: Temporal distribution and other characteristics of new particle formation events in an urban environment, Environ. Pollut., 233, 552–560, https://doi.org/10.1016/j.envpol.2017.10.102, 2018.

Ren, J., Chen, L., Fan, T., Liu, J., Jiang, S., and Zhang, F.: The NPF Effect on CCN Number Concentrations: A Review and Re-Evaluation of Observations From 35 Sites Worldwide, Geophys. Res. Lett., 48, e2021GL095190, https://doi.org/10.1029/2021GL095190, 2021.

Rivellini, L.-H., Chiapello, I., Tison, E., Fourmentin, M., Féron, A., Diallo, A., N'Diaye, T., Goloub, P., Canonaco, F., Prévôt, A. S. H., and Riffault, V.: Chemical characterization and source apportionment of submicron aerosols measured in Senegal during the 2015 SHADOW campaign, Atmos. Chem. Phys., 17, 10291–10314, https://doi.org/10.5194/acp-17-10291-2017, 2017.

Rodríguez, S., Van Dingenen, R., Putaud, J.-P., Martins-Dos Santos, S., and Roselli, D.: Nucleation and growth of new particles in the rural atmosphere of Northern Italy – relationship to air quality monitoring, Atmos. Environ., 39, 6734–6746, https://doi.org/10.1016/j.atmosenv.2005.07.036, 2005.

Rodríguez, S., Cuevas, E., González, Y., Ramos, R., Romero, P. M., Pérez, N., Querol, X., and Alastuey, A.: Influence of sea breeze circulation and road traffic emissions on the relationship between particle number, black carbon, PM1, PM2.5 and PM2.5–10 concentrations in a coastal city, Atmos. Environ., 42, 6523–6534, https://doi.org/10.1016/j.atmosenv.2008.04.022, 2008.

Roig Rodelas, R., Chakraborty, A., Perdrix, E., Tison, E., and Riffault, V.: Real-time assessment of wintertime organic aerosol characteristics and sources at a suburban site in northern France, Atmos. Environ., 203, 48–61, https://doi.org/10.1016/j.atmosenv.2019.01.035, 2019.

Rolph, G., Stein, A., and Stunder, B.: Real-time Environmental Applications and Display sYstem: READY, Environ. Modell. Softw., 95, 210–228, https://doi.org/10.1016/j.envsoft.2017.06.025, 2017.

Rose, C., Sellegri, K., Freney, E., Dupuy, R., Colomb, A., Pichon, J.-M., Ribeiro, M., Bourianne, T., Burnet, F., and Schwarzenboeck, A.: Airborne measurements of new particle formation in the free troposphere above the Mediterranean Sea during the HYMEX campaign, Atmos. Chem. Phys., 15, 10203–10218, https://doi.org/10.5194/acp-15-10203-2015, 2015a.

Rose, C., Sellegri, K., Asmi, E., Hervo, M., Freney, E., Colomb, A., Junninen, H., Duplissy, J., Sipilä, M., Kontkanen, J., Lehtipalo, K., and Kulmala, M.: Major contribution of neutral clusters to new particle formation at the interface between the boundary layer and the free troposphere, Atmos. Chem. Phys., 15, 3413–3428, https://doi.org/10.5194/acp-15-3413-2015, 2015b.

Rose, C., Sellegri, K., Moreno, I., Velarde, F., Ramonet, M., Weinhold, K., Krejci, R., Andrade, M., Wiedensohler, A., Ginot, P., and Laj, P.: CCN production by new particle formation in the free troposphere, Atmos. Chem. Phys., 17, 1529–1541, https://doi.org/10.5194/acp-17-1529-2017, 2017.

Rose, C., Collaud Coen, M., Andrews, E., Lin, Y., Bossert, I., Lund Myhre, C., Tuch, T., Wiedensohler, A., Fiebig, M., Aalto, P., Alastuey, A., Alonso-Blanco, E., Andrade, M., Artíñano, B., Arsov, T., Baltensperger, U., Bastian, S., Bath, O., Beukes, J. P., Brem, B. T., Bukowiecki, N., Casquero-Vera, J. A., Conil, S., Eleftheriadis, K., Favez, O., Flentje, H., Gini, M. I., Gómez-Moreno, F. J., Gysel-Beer, M., Hallar, A. G., Kalapov, I., Kalivitis, N., Kasper-Giebl, A., Keywood, M., Kim, J. E., Kim, S.-W., Kristensson, A., Kulmala, M., Lihavainen, H., Lin, N.-H., Lyamani, H., Marinoni, A., Martins Dos Santos, S., Mayol-Bracero, O. L., Meinhardt, F., Merkel, M., Metzger, J.-M., Mihalopoulos, N., Ondracek, J., Pandolfi, M., Pérez, N., Petäjä, T., Petit, J.-E., Picard, D., Pichon, J.-M., Pont, V., Putaud, J.-P., Reisen, F., Sellegri, K., Sharma, S., Schauer, G., Sheridan, P., Sherman, J. P., Schwerin, A., Sohmer, R., Sorribas, M., Sun, J., Tulet, P., Vakkari, V., van Zyl, P. G., Velarde, F., Villani, P., Vratolis, S., Wagner, Z., Wang, S.-H., Weinhold, K., Weller, R., Yela, M., Zdimal, V., and Laj, P.: Seasonality of the particle number concentration and size distribution: a global analysis retrieved from the network of Global Atmosphere Watch (GAW) near-surface observatories, Atmos. Chem. Phys., 21, 17185–17223, https://doi.org/10.5194/acp-21-17185-2021, 2021.

Salimi, F., Rahman, Md. M., Clifford, S., Ristovski, Z., and Morawska, L.: Nocturnal new particle formation events in

urban environments, Atmos. Chem. Phys., 17, 521–530, https://doi.org/10.5194/acp-17-521-2017, 2017.

Salma, I., Németh, Z., Kerminen, V.-M., Aalto, P., Nieminen, T., Weidinger, T., Molnár, Á., Imre, K., and Kulmala, M.: Regional effect on urban atmospheric nucleation, Atmos. Chem. Phys., 16, 8715–8728, https://doi.org/10.5194/acp-16-8715-2016, 2016.

Salma, I., Varga, V., and Németh, Z.: Quantification of an atmospheric nucleation and growth process as a single source of aerosol particles in a city, Atmos. Chem. Phys., 17, 15007–15017, https://doi.org/10.5194/acp-17-15007-2017, 2017.

Sandradewi, J., Prévôt, A. S. H., Szidat, S., Perron, N., Alfarra, M. R., Lanz, V. A., Weingartner, E., and Baltensperger, U.: Using aerosol light absorption measurements for the quantitative determination of wood burning and traffic emission contributions to particulate matter, Environ. Sci. Technol., 42, 3316–3323, 2008.

Sebastian, M., Kanawade, V. P., Soni, V. K., Asmi, E., Westervelt, Daniel. M., Vakkari, V., Hyvärinen, A.-P., Pierce, J. R., and Hooda, R. K.: New Particle Formation and Growth to Climate-Relevant Aerosols at a Background Remote Site in the Western Himalaya, J. Geophys. Res.-Atmos., 126, e2020JD033267, https://doi.org/10.1029/2020JD033267, 2021.

Seinfeld, J. H. and Pandis, S. N.: Atmospheric Chemistry and Physics: From Air Pollution to Climate Change, Wiley, ISBN 9780471720188, 2016.

Sellegri, K., Rose, C., Marinoni, A., Lupi, A., Wiedensohler, A., Andrade, M., Bonasoni, P., and Laj, P.: New Particle Formation: A Review of Ground-Based Observations at Mountain Research Stations, Atmosphere, 10, 493, https://doi.org/10.3390/atmos10090493, 2019.

Shukla, K. K., Niranjan Kumar, K., Phanikumar, D. V., Newsom, R. K., Kotamarthi, V. R., Ouarda, T. B. M. J., and Ratnam, M. V.: Identification of the cloud base height over the central Himalayan region: Intercomparison of Ceilometer and Doppler Lidar, Atmos. Meas. Tech. Discuss. [preprint], https://doi.org/10.5194/amt-2016-162, 2016.

Sogacheva, L., Maso, M. D., Kerminen, V. M., and Kulmala, M.: Probability of nucleation events and aerosol particle concentration in different air mass types arriving at Hyytiala southern Finland, based on back trajectories analysis, Boreal Environ. Res., 10, 479–491, 2005.

Sogacheva, L., Hamed, A., Facchini, M. C., Kulmala, M., and Laaksonen, A.: Relation of air mass history to nucleation events in Po Valley, Italy, using back trajectories analysis, Atmos. Chem. Phys., 7, 839–853, https://doi.org/10.5194/acp-7-839-2007, 2007.

Spracklen, D. V., Carslaw, K. S., Kulmala, M., Kerminen, V.-M., Mann, G. W., and Sihto, S.-L.: The contribution of boundary layer nucleation events to total particle concentrations on regional and global scales, Atmos. Chem. Phys., 6, 5631–5648, https://doi.org/10.5194/acp-6-5631-2006, 2006.

Stein, A. F., Draxler, R. R., Rolph, G. D., Stunder, B. J. B., Cohen, M. D., and Ngan, F.: NOAA's HYSPLIT Atmospheric Transport and Dispersion Modeling System, B. Am. Meteorol. Soc., 96, 2059–2077, https://doi.org/10.1175/BAMS-D-14-00110.1, 2015.

Tillmann, R., Hallquist, M., Jonsson, Å. M., Kiendler-Scharr, A., Saathoff, H., Iinuma, Y., and Mentel, Th. F.: Influence of relative humidity and temperature on the production of pinonaldehyde and OH radicals from the ozonolysis of α-pinene, Atmos. Chem. Phys., 10, 7057–7072, https://doi.org/10.5194/acp-10-7057-2010, 2010.

Tuch, T. M., Herbarth, O., Franck, U., Peters, A., Wehner, B., Wiedensohler, A., and Heintzenberg, J.: Weak correlation of ultrafine aerosol particle concentrations < 800 nm between two sites within one city, J. Expo. Sci. Env. Epid., 16, 486–490, https://doi.org/10.1038/sj.jes.7500469, 2006.

Tunved, P., Hansson, H.-C., Kerminen, V.-M., Ström, J., Dal Maso, M., Lihavainen, H., Viisanen, Y., Aalto, P. P., Komppula, M., and Kulmala, M.: High natural aerosol loading over boreal forests, Science, 312, 261–263, https://doi.org/10.1126/science.1123052, 2006.

Uusitalo, H., Kontkanen, J., Ylivinkka, I., Ezhova, E., Demakova, A., Arshinov, M., Belan, B. D., Davydov, D., Ma, N., Petäjä, T., Wiedensohler, A., Kulmala, M., and Nieminen, T.: Occurrence of new particle formation events in Siberian and Finnish boreal forest, Atmos. Chem. Phys. Discuss. [preprint], https://doi.org/10.5194/acp-2021-530, in review, 2021.

Velazquez-Garcia, Crumeyrolle, S., Brito, J., Tison, E., Bourrianne, E., Chiapello, I., and Riffault, V.: Deriving composition-dependent aerosol absorption, scattering and extinction mass efficiencies from multi-annual high time resolution observations in Northern France, Atmos. Environ., submitted, 2022.

Villani, P., Picard, D., Marchand, N., and Laj, P.: Design and validation of a 6-volatility tandem differential mobility analyzer (VTDMA), Aerosol Sci. Tech., 41, 898–906, https://doi.org/10.1080/02786820701534593, 2007.

Wang, M., Kong, W., Marten, R., He, X.-C., Chen, D., Pfeifer, J., Heitto, A., Kontkanen, J., Dada, L., Kürten, A., Yli-Juuti, T., Manninen, H. E., Amanatidis, S., Amorim, A., Baalbaki, R., Baccarini, A., Bell, D. M., Bertozzi, B., Bräkling, S., Brilke, S., Murillo, L. C., Chiu, R., Chu, B., De Menezes, L.-P., Duplissy, J., Finkenzeller, H., Carracedo, L. G., Granzin, M., Guida, R., Hansel, A., Hofbauer, V., Krechmer, J., Lehtipalo, K., Lamkaddam, H., Lampimäki, M., Lee, C. P., Makhmutov, V., Marie, G., Mathot, S., Mauldin, R. L., Mentler, B., Müller, T., Onnela, A., Partoll, E., Petäjä, T., Philippov, M., Pospisilova, V., Ranjithkumar, A., Rissanen, M., Rörup, B., Scholz, W., Shen, J., Simon, M., Sipilä, M., Steiner, G., Stolzenburg, D., Tham, Y. J., Tomé, A., Wagner, A. C., Wang, D. S., Wang, Y., Weber, S. K., Winkler, P. M., Wlasits, P. J., Wu, Y., Xiao, M., Ye, Q., Zauner-Wieczorek, M., Zhou, X., Volkamer, R., Riipinen, I., Dommen, J., Curtius, J., Baltensperger, U., Kulmala, M., Worsnop, D. R., Kirkby, J., Seinfeld, J. H., El-Haddad, I., Flagan, R. C., and Donahue, N. M.: Rapid growth of new atmospheric particles by nitric acid and ammonia condensation, Nature, 581, 184–189, https://doi.org/10.1038/s41586-020-2270-4, 2020.

Wang, Z., Wu, Z., Yue, D., Shang, D., Guo, S., Sun, J., Ding, A., Wang, L., Jiang, J., Guo, H., Gao, J., Cheung, H. C., Morawska, L., Keywood, M., and Hu, M.: New particle formation in China: Current knowledge and further directions, Sci. Total Environ., 577, 258–266, https://doi.org/10.1016/j.scitotenv.2016.10.177, 2017.

Wang, Z. B., Hu, M., Wu, Z. J., Yue, D. L., Zheng, J., Zhang, R. Y., Pei, X. Y., Paasonen, P., Dal Maso, M., Boy, M., and Wiedensohler, A.: Investigation of the connections between atmospheric new particle formation and organics at an urban site of Beijing, Atmos. Chem. Phys. Discuss., 13, 3419–3450, https://doi.org/10.5194/acpd-13-3419-2013, 2013.

Wehner, B. and Wiedensohler, A.: Long term measurements of submicrometer urban aerosols: statistical analysis for correlations with meteorological conditions and trace gases, Atmos. Chem. Phys., 3, 867–879, https://doi.org/10.5194/acp-3-867-2003, 2003.

Xiao, S., Wang, M. Y., Yao, L., Kulmala, M., Zhou, B., Yang, X., Chen, J. M., Wang, D. F., Fu, Q. Y., Worsnop, D. R., and Wang, L.: Strong atmospheric new particle formation in winter in urban Shanghai, China, Atmos. Chem. Phys., 15, 1769–1781, https://doi.org/10.5194/acp-15-1769-2015, 2015.

Yao, L., Garmash, O., Bianchi, F., Zheng, J., Yan, C., Kontkanen, J., Junninen, H., Mazon, S. B., Ehn, M., Paasonen, P., Sipilä, M., Wang, M., Wang, X., Xiao, S., Chen, H., Lu, Y., Zhang, B., Wang, D., Fu, Q., Geng, F., Li, L., Wang, H., Qiao, L., Yang, X., Chen, J., Kerminen, V.-M., Petäjä, T., Worsnop, D. R., Kulmala, M., and Wang, L.: Atmospheric new particle formation from sulfuric acid and amines in a Chinese megacity, Science, 361, 278–281, https://doi.org/10.1126/science.aao4839, 2018.

Yli-Juuti, T., Nieminen, T., Hirsikko, A., Aalto, P. P., Asmi, E., Hõrrak, U., Manninen, H. E., Patokoski, J., Dal Maso, M., Petäjä, T., Rinne, J., Kulmala, M., and Riipinen, I.: Growth rates of nucleation mode particles in Hyytiälä during 2003−2009: variation with particle size, season, data analysis method and ambient conditions, Atmos. Chem. Phys., 11, 12865–12886, https://doi.org/10.5194/acp-11-12865-2011, 2011.